The Characterization of the Gamma-Ray Signal from the Central Milky Way: A Compelling Case for Annihilating Dark Matter

Tansu Daylan,[1] Douglas P. Finkbeiner,[1,2] Dan Hooper,[3,4] Tim Linden,[5]
Stephen K. N. Portillo,[2] Nicholas L. Rodd,[6] and Tracy R. Slatyer[6,7]

[1]*Department of Physics, Harvard University, Cambridge, MA*
[2]*Harvard-Smithsonian Center for Astrophysics, Cambridge, MA*
[3]*Fermi National Accelerator Laboratory, Theoretical Astrophysics Group, Batavia, IL*
[4]*University of Chicago, Department of Astronomy and Astrophysics, Chicago, IL*
[5]*University of Chicago, Kavli Institute for Cosmological Physics, Chicago, IL*
[6]*Center for Theoretical Physics, Massachusetts Institute of Technology, Boston, MA*
[7]*School of Natural Sciences, Institute for Advanced Study, Princeton, NJ*

Past studies have identified a spatially extended excess of ∼1-3 GeV gamma rays from the region surrounding the Galactic Center, consistent with the emission expected from annihilating dark matter. We revisit and scrutinize this signal with the intention of further constraining its characteristics and origin. By applying cuts to the *Fermi* event parameter CTBCORE, we suppress the tails of the point spread function and generate high resolution gamma-ray maps, enabling us to more easily separate the various gamma-ray components. Within these maps, we find the GeV excess to be robust and highly statistically significant, with a spectrum, angular distribution, and overall normalization that is in good agreement with that predicted by simple annihilating dark matter models. For example, the signal is very well fit by a 31-40 GeV dark matter particle annihilating to $b\bar{b}$ with an annihilation cross section of $\sigma v = (1.4 - 2.0) \times 10^{-26}$ cm^3/s (normalized to a local dark matter density of 0.3 GeV/cm^3). Furthermore, we confirm that the angular distribution of the excess is approximately spherically symmetric and centered around the dynamical center of the Milky Way (within ∼0.05° of Sgr A*), showing no sign of elongation along or perpendicular to the Galactic Plane. The signal is observed to extend to at least $\simeq 10°$ from the Galactic Center, disfavoring the possibility that this emission originates from millisecond pulsars.

PACS numbers: 95.85.Pw, 98.70.Rz, 95.35.+d; FERMILAB-PUB-14-032-A, MIT-CTP 4533

I. INTRODUCTION

Weakly interacting massive particles (WIMPs) are a leading class of candidates for the dark matter of our universe. If the dark matter consists of such particles, then their annihilations are predicted to produce potentially observable fluxes of energetic particles, including gamma rays, cosmic rays, and neutrinos. Of particular interest are gamma rays from the region of the Galactic Center which, due to its proximity and high dark matter density, is expected to be the brightest source of dark matter annihilation products on the sky, hundreds of times brighter than the most promising dwarf spheroidal galaxies.

Over the past few years, several groups analyzing data from the *Fermi* Gamma-Ray Space Telescope have reported the detection of a gamma-ray signal from the inner few degrees around the Galactic Center (corresponding to a region several hundred parsecs in radius), with a spectrum and angular distribution compatible with that anticipated from annihilating dark matter particles [1–7]. More recently, this signal was shown to also be present throughout the larger Inner Galaxy region, extending kiloparsecs from the center of the Milky Way [8, 9]. While the spectrum and morphology of the Galactic Center and Inner Galaxy signals have been shown to be compatible with that predicted from the annihilations of an approximately 30-40 GeV WIMP annihilating to quarks (or a ∼7-10 GeV WIMP annihilating significantly to tau leptons), other explanations have also been proposed. In particular, it has been argued that if our galaxy's central stellar cluster contains several thousand unresolved millisecond pulsars, they might be able to account for the emission observed from the Galactic Center [2, 4–7, 10]. The realization that this signal extends well beyond the boundaries of the central stellar cluster [8, 9] disfavors such interpretations, however. In particular, pulsar population models capable of producing the observed emission from the Inner Galaxy invariably predict that *Fermi* should have resolved a much greater number of such objects. Accounting for this constraint, Ref. [11] concluded that no more than ∼5-10% of the anomalous gamma-ray emission from the Inner Galaxy can originate from pulsars. Furthermore, while it has been suggested that the Galactic Center signal might result from cosmic-ray interactions with gas [2, 4–6], the analyses of Refs. [12] and [13] find that measured distributions of gas provide a poor fit to the morphology of the observed signal. It also appears implausible that such processes could account for the more spatially extended emission observed from throughout the Inner Galaxy.

In this study, we revisit the anomalous gamma-ray emission from the Galactic Center and the Inner Galaxy regions and scrutinize the *Fermi* data in an effort to constrain and characterize this signal more definitively, with the ultimate goal being to confidently determine its origin. One way in which we expand upon previous work

is by selecting photons based on the value of the *Fermi* event parameter CTBCORE. Through the application of this cut, we select only those events with more reliable directional reconstruction, allowing us to better separate the various gamma-ray components, and to better limit the degree to which emission from the Galactic Disk leaks into the regions studied in our Inner Galaxy analysis. After applying this cut, we are able to produce a much more robust determination of the spectrum and morphology of the Inner Galaxy and the Galactic Center signals. We go on to apply a number of tests to this data, and determine that the anomalous emission in question agrees well with that predicted from the annihilations of a 31-40 GeV WIMP annihilating mostly to b quarks (or a somewhat lower mass WIMP if its annihilations proceed to first or second generation quarks). Our results now appear to disfavor the previously considered 7-10 GeV mass window in which the dark matter annihilates significantly to tau leptons [2, 4, 6–8] (the analysis of Ref. [6] also disfavored this scenario). The morphology of the signal is consistent with spherical symmetry, and strongly disfavors any significant elongation along or perpendicular to the Galactic Plane. The emission decreases with the distance to the Galactic Center at a rate consistent with a dark matter halo profile which scales as $\rho \propto r^{-\gamma}$, with $\gamma \approx 1.1-1.3$. The signal can be identified out to angles of $\simeq 10^{\circ}$ from the Galactic Center, beyond which systematic uncertainties related to the Galactic diffuse model become significant. The annihilation cross section required to normalize the observed signal is $\sigma v \sim 2 \times 10^{-26}$ cm^3/s, in good agreement with that predicted for dark matter in the form of a simple thermal relic.

The remainder of this article is structured as follows. In the following section, we review the calculation of the spectrum and angular distribution of gamma rays predicted from annihilating dark matter. In Sec. III, we describe the event selection used in our analysis, including the application of cuts on the *Fermi* event parameter CTBCORE. In Secs. IV and V, we describe our analyses of the Inner Galaxy and Galactic Center regions, respectively. In each of these analyses, we observe a significant gamma-ray excess, with a spectrum and morphology in good agreement with that predicted from annihilating dark matter. We further investigate the angular distribution of this emission in Sec. VI, and discuss the dark matter interpretation of this signal in Sec. VII. In Sec. VIII we discuss the implications of these observations, and offer predictions for other upcoming observations. Finally, we summarize our results and conclusions in Sec. IX. In the paper's appendices, we include supplemental material intended for those interested in further details of our analysis.

II. GAMMA RAYS FROM DARK MATTER ANNIHILATIONS IN THE HALO OF THE MILKY WAY

Dark matter searches using gamma-ray telescopes have a number of advantages over other indirect detection strategies. Unlike signals associated with cosmic rays (electrons, positrons, antiprotons, etc.), gamma rays are not deflected by magnetic fields. Furthermore, gamma-ray energy losses are negligible on galactic scales. As a result, gamma-ray telescopes can potentially acquire both spectral and spatial information, unmolested by astrophysical effects.

The flux of gamma rays generated by annihilating dark matter particles, as a function of the direction observed, ψ, is given by:

$$\Phi(E_\gamma, \psi) = \frac{\sigma v}{8\pi m_X^2} \frac{\mathrm{d}N_\gamma}{\mathrm{d}E_\gamma} \int_{\mathrm{los}} \rho^2(r)\, \mathrm{d}l, \qquad (1)$$

where m_X is the mass of the dark matter particle, σv is the annihilation cross section (times the relative velocity of the particles), dN_γ/dE_γ is the gamma-ray spectrum produced per annihilation, and the integral of the density squared is performed over the line-of-sight (los). Although N-body simulations lead us to expect dark matter halos to exhibit some degree of triaxiality (see [14] and references therein), the Milky Way's dark matter distribution is generally assumed to be approximately spherically symmetric, allowing us to describe the density as a function of only the distance from the Galactic Center, r. Throughout this study, we will consider dark matter distributions described by a generalized Navarro-Frenk-White (NFW) halo profile [15, 16]:

$$\rho(r) = \rho_0 \frac{(r/r_s)^{-\gamma}}{(1 + r/r_s)^{3-\gamma}}. \qquad (2)$$

Throughout this paper, we adopt a scale radius of $r_s = 20$ kpc, and select ρ_0 such that the local dark matter density (at 8.5 kpc from the Galactic Center) is 0.3 GeV/cm^3, consistent with dynamical constraints [17, 18]. Although dark matter-only simulations generally favor inner slopes near the canonical NFW value ($\gamma = 1$) [19, 20], baryonic effects are expected to have a non-negligible impact on the dark matter distribution within the inner $\sim$10 kiloparsecs of the Milky Way [21–31]. The magnitude and direction of such baryonic effects, however, are currently a topic of debate. With this in mind, we remain agnostic as to the value of the inner slope, and take γ to be a free parameter.

In the left frame of Fig. 1, we plot the density of dark matter as a function of r for several choices of the halo profile. Along with generalized NFW profiles using three values of the inner slope (γ=1.0, 1.2, 1.4), we also show for comparison the results for an Einasto profile (with $\alpha = 0.17$) [32]. In the right frame, we plot the value of the integral in Eq. 1 for the same halo profiles, denoted

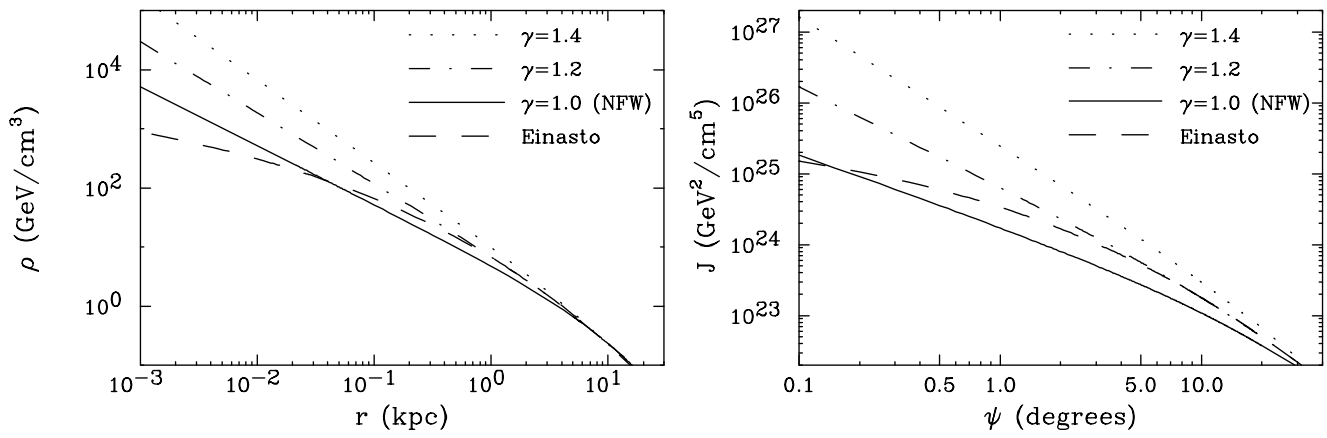

FIG. 1: Left frame: The dark matter density as a function of the distance to the Galactic Center, for several halo profiles, each normalized such that $\rho = 0.3$ GeV/cm^3 at $r = 8.5$ kpc. Right frame: The line-of-sight integral of the density squared, as defined in Eq. 3, for the same set of halo profiles, as a function of the angular distance from the Galactic Center, ψ.

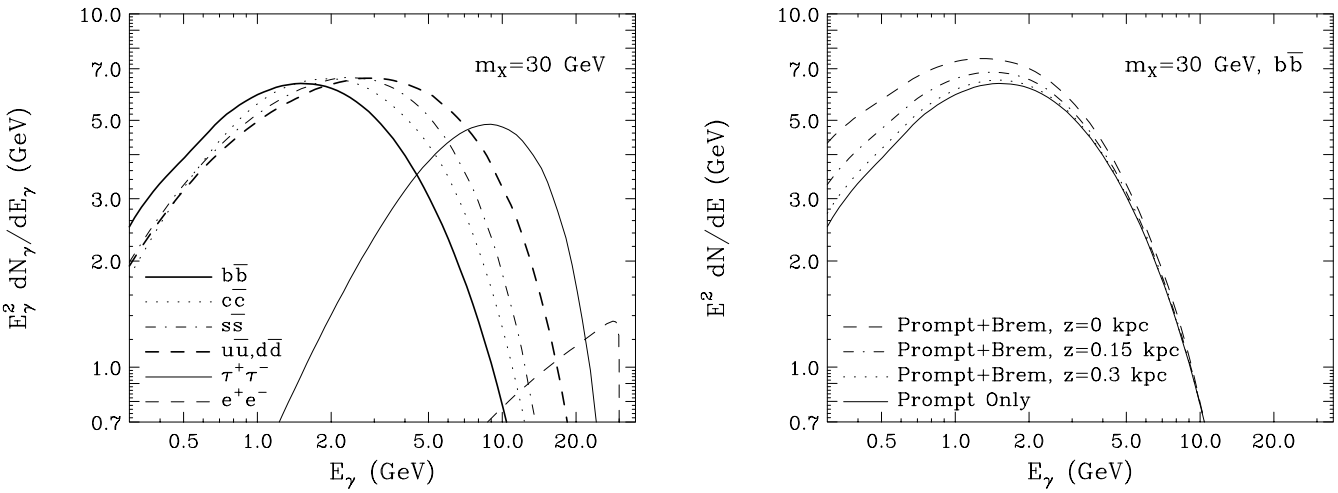

FIG. 2: Left frame: The spectrum of gamma rays produced per dark matter annihilation for a 30 GeV WIMP mass and a variety of annihilation channels. Right frame: An estimate for the bremsstrahlung emission from the electrons produced in dark matter annihilations taking place near the Galactic Center, for the case of a 30 GeV WIMP annihilating to $b\bar{b}$. At $|z| \lesssim 0.3$ kpc ($|b| \lesssim 2^\circ$) and at energies below ∼1-2 GeV, bremsstrahlung could potentially contribute non-negligibly. See text for details.

by the quantity, $J(\psi)$:

$$J(\psi) = \int_{\rm los} \rho^2(r)\, dl, \qquad (3)$$

where ψ is the angle observed away from the Galactic Center. In the NFW case (with $\gamma = 1$), for example, the value of J averaged over the inner degree around the Galactic Center exceeds that of the most promising dwarf spheroidal galaxies by a factor of ∼50 [33]. If the Milky Way's dark matter halo is contracted by baryons or is otherwise steeper than predicted by NFW, this ratio could easily be $\sim 10^3$ or greater.

The spectrum of gamma rays produced per dark matter annihilation, dN_γ/dE_γ, depends on the mass of the dark matter particle and on the types of particles produced in this process. In the left frame of Fig. 2, we plot dN_γ/dE_γ for the case of a 30 GeV WIMP mass, and for a variety of annihilation channels (as calculated using PYTHIA [34], except for the e^+e^- case, for which the final state radiation was calculated analytically [35, 36]). In each case, a distinctive bump-like feature appears, although at different energies and with different widths, depending on the final state.

In addition to prompt gamma rays, dark matter annihilations can produce electrons and positrons which subsequently generate gamma rays via inverse Compton and bremsstrahlung processes. For dark matter annihilations taking place near the Galactic Plane, the low-energy gamma-ray spectrum can receive a non-negligible contribution from bremsstrahlung. In the right frame of Fig. 2, we plot the gamma-ray spectrum from dark matter (per annihilation), including an estimate for the

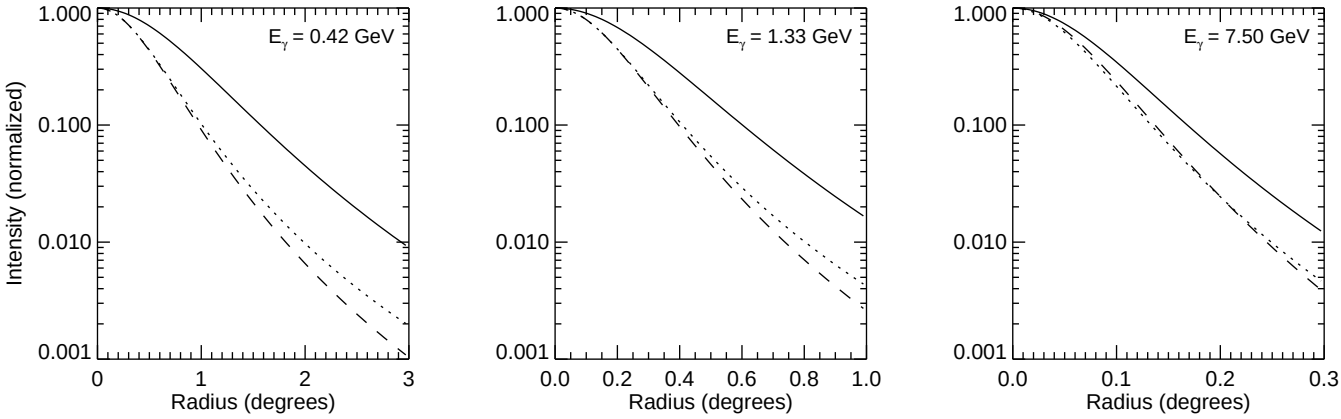

FIG. 3: The point spread function (PSF) of the *Fermi* Gamma-Ray Space Telescope, for front-converting, Ultraclean class events. The solid lines represent the PSF for the full dataset, using the *Fermi* Collaboration's default cuts on the parameter CTBCORE. The dotted and dashed lines, in contrast, denote the PSFs for the top two quartiles (Q2) and top quartile (Q1) of these events, respectively, as ranked by CTBCORE. See text for details.

bremsstrahlung contribution. In estimating the contribution from bremsstrahlung, we neglect diffusion, but otherwise follow the calculation of Ref. [37]. In particular, we consider representative values of $\langle B \rangle = 10\,\mu$G for the magnetic field, and 10 eV/cm^3 for the radiation density throughout the region of the Galactic Center. For the distribution of gas, we adopt a density of 10 particles per cm^3 near the Galactic Plane ($z = 0$), with a dependence on z given by $\exp(-|z|/0.15\,\mathrm{kpc})$. Within $\sim 1^\circ - 2^\circ$ of the Galactic Plane, we find that bremsstrahlung could potentially contribute non-negligibly to the low energy ($\lesssim$1–2 GeV) gamma-ray spectrum from annihilating dark matter.

III. MAKING HIGHER RESOLUTION GAMMA-RAY MAPS WITH CTBCORE

In most analyses of *Fermi* data, one makes use of all of the events within a given class (Transient, Source, Clean, or Ultraclean). Each of these event classes reflects a different trade-off between the effective area and the efficiency of cosmic-ray rejection. Higher quality event classes also allow for somewhat greater angular resolution (as quantified by the point spread function, PSF). The optimal choice of event class for a given analysis depends on the nature of the signal and background in question. The Ultraclean event class, for example, is well suited to the study of large angular regions, and to situations where the analysis is sensitive to spectral features that might be caused by cosmic ray backgrounds. The Transient event class, in contrast, is best suited for analyses of short duration events, with little background. Searches for dark matter annihilation products from the Milky Way's halo significantly benefit from the high background rejection and (slightly) better angular resolution of the Ultraclean class and thus can potentially fall into the former category.

As a part of event reconstruction, the *Fermi* Collaboration estimates the accuracy of the reconstructed direction of each event. Inefficiencies and inactive regions within the detector reduce the quality of the information available for certain events. Factors such as whether an event is front-converting or back-converting, whether there are multiple tracks that can be combined into a vertex, and the amount of energy deposited into the calorimeter each impact the reliability of the reconstructed direction [38].

In their most recent public data releases, the *Fermi* Collaboration has begun to include a greater body of information about each event, including a value for the parameter CTBCORE, which quantifies the reliability of the directional reconstruction. By selecting only events with a high value of CTBCORE, one can reduce the tails of the PSF, although at the expense of effective area [38].

For this study, we have created a set of new event classes by increasing the CTBCORE cut from the default values used by the *Fermi* Collaboration. To accomplish this, we divided all front-converting, Ultraclean events (Pass 7, Reprocessed) into quartiles, ranked by CTBCORE. Those events in the top quartile make up the event class Q1, while those in the top two quartiles make up Q2, etc. For each new event class, we calibrate the on-orbit PSF [39] using the Geminga pulsar. Taking advantage of Geminga's pulsation, we remove the background by taking the difference between the on-phase and off-phase images. We fit the PSF in each energy bin by a single King function, and smooth the overall PSF with energy. This procedure is effective up to 10 GeV, above which we become statistics limited and do not apply any additional cuts to CTBCORE. We also rescale *Fermi*'s effective area according to the fraction of events that are removed by the CTBCORE cut, as a function of energy and incidence angle.

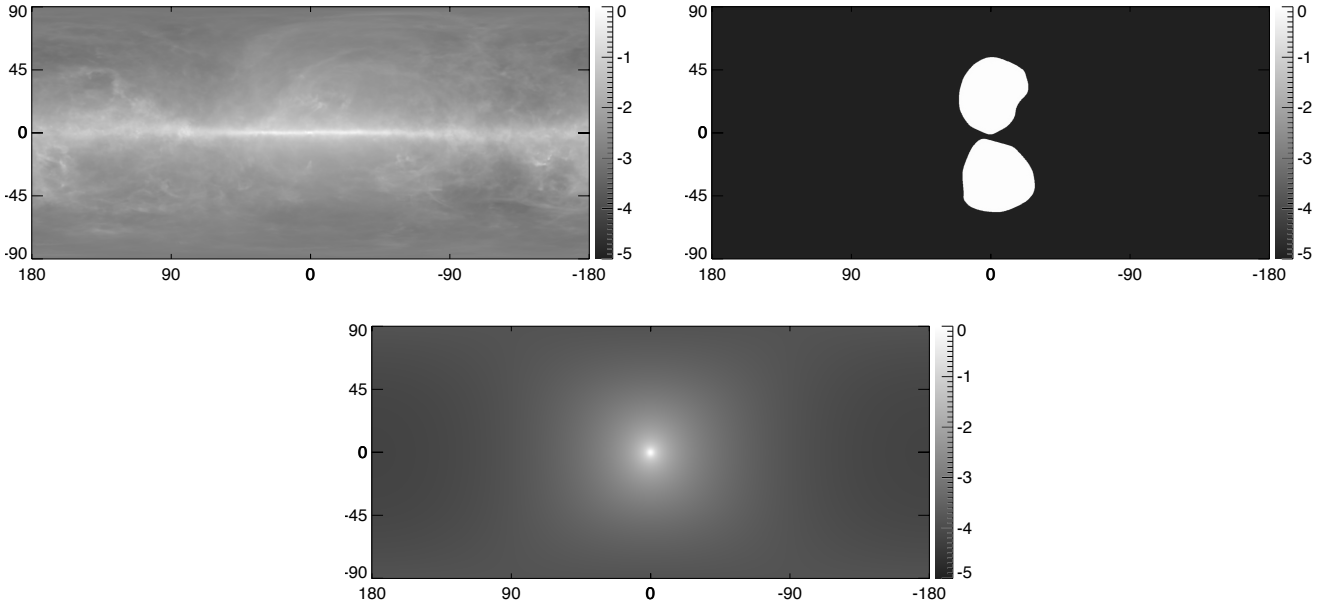

FIG. 4: The spatial templates (in galactic coordinates) for the Galactic diffuse model (upper left), the *Fermi* bubbles (upper right), and dark matter annihilation products (lower), as used in our Inner Galaxy analysis. The scale is logarithmic (base 10), normalized to the brightest point in each map. The diffuse model template is shown as evaluated at 2 GeV, and the dark matter template corresponds to a generalized NFW profile with an inner slope of $\gamma = 1.3$.

These cuts on CTBCORE have a substantial impact on *Fermi*'s PSF, especially at low energies. In Fig. 3, we show the PSF for front-converting, Ultraclean events, at three representative energies, for different cuts on CTBCORE (all events, Q2, and Q1). Such a cut can be used to mitigate the leakage of astrophysical emission from the Galactic Plane and point sources into our regions of interest. This leakage is most problematic at low energies, where the PSF is quite broad and where the CTBCORE cut has the greatest impact. These new event classes and their characterization will be further detailed in an upcoming paper, which will be accompanied by a data release of all-sky maps for each class, and the instrument response function files necessary for use with the *Fermi* Science Tools [40].

Throughout the remainder of this study, we will employ the Q2 event class, corresponding to the top 50% (by CTBCORE) of *Fermi*'s front-converting, Ultraclean photons, except at energies above 10 GeV, where we do not apply any additional cuts to CTBCORE.

IV. THE INNER GALAXY

In this section, we follow the procedure previously pursued in Ref. [8] (see also Refs. [41, 42]) to study the gamma-ray emission from the Inner Galaxy. We use the term "Inner Galaxy" to denote the region of the sky that lies within several tens of degrees around the Galactic Center, excepting the Galactic Plane itself ($|b| < 1^\circ$), which we mask in this portion of our analysis.

Throughout our analysis, we make use of the Pass 7 (V15) reprocessed data taken between August 4, 2008 and December 5, 2013, using only front-converting, Ultraclean class events which pass the Q2 CTBCORE cut as described in Sec. III. We also apply standard cuts to ensure data quality (zenith angle $< 100^\circ$, instrumental rocking angle $< 52^\circ$, `DATA_QUAL` $= 1$, `LAT_CONFIG`$=1$). Using this data set, we have generated a map of the gamma-ray sky, smoothed to 2 degrees full-width-half-maximum. We apply the point source subtraction method described in Ref. [42], using the 1FGL catalogue and masking out the 200 brightest sources. We then performed a pixel-based maximum likelihood analysis on the map, fitting the data in each energy bin to a sum of spatial templates. These templates consist of: 1) the *Fermi* Collaboration `p6v11` Galactic diffuse model (which we refer to as the Pass 6 Diffuse Model),[1] 2) an isotropic map, intended to account for the extragalactic gamma-ray background and residual cosmic-ray contamination, and 3) a uniform-brightness spatial template coincident with the features known as the *Fermi* Bubbles, as described in Ref. [42]. In addition to these three back-

[1] Unlike more recently released Galactic diffuse models, the `p6v11` diffuse model does not include a component corresponding to the *Fermi* Bubbles. By using this model, we are free to fit the *Fermi* Bubbles component independently. See Appendix D for a discussion of the impact of varying the diffuse model.

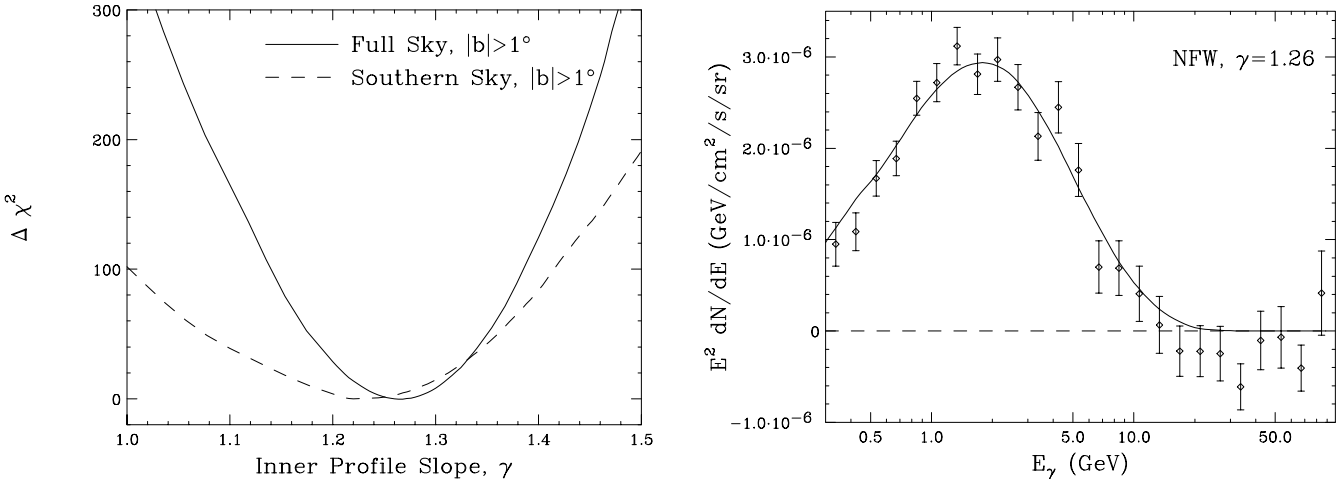

FIG. 5: Left frame: The value of the formal statistical $-2\Delta \ln \mathcal{L}$ (referred to as $\Delta\chi^2$) extracted from the likelihood fit, as a function of the inner slope of the dark matter halo profile, γ. Results are shown using gamma-ray data from the full sky (solid line) and only the southern sky (dashed line). Unlike in the analysis of Ref. [8], we do not find any large north-south asymmetry in the preferred value of γ. Right frame: The spectrum of the dark matter component, for a template corresponding to a generalized NFW halo profile with an inner slope of $\gamma = 1.26$ (normalized to the flux at an angle of 5° from the Galactic Center). Shown for comparison (solid line) is the spectrum predicted from a 35.25 GeV dark matter particle annihilating to $b\bar{b}$ with a cross section of $\sigma v = 1.7 \times 10^{-26}$ cm^3/s $\times [(0.3\,\mathrm{GeV/cm^3})/\rho_{\mathrm{local}}]^2$.

ground templates, we include an additional dark matter template, motivated by the hypothesis that the previously reported gamma-ray excess originates from annihilating dark matter. In particular, our dark matter template is taken to be proportional to the line-of-sight integral of the dark matter density squared, $J(\psi)$, for a generalized NFW density profile (see Eqs. 2–3). The spatial morphology of the Galactic diffuse model (as evaluated at 2 GeV), *Fermi* Bubbles, and dark matter templates are each shown in Fig. 4.

As found in previous studies [8, 9], the inclusion of the dark matter template dramatically improves the quality of the fit to the *Fermi* data. For the best-fit spectrum and halo profile, we find that the inclusion of the dark matter template improves the formal fit by $\Delta\chi^2 \simeq 1672$, corresponding to a statistical preference greater than 40σ. When considering this enormous statistical significance, one should keep in mind that in addition to statistical errors there is a degree of unavoidable and unaccounted-for systematic error, in that neither model (with or without a dark matter component) is a "good fit" in the sense of describing the sky to the level of Poisson noise. That being said, the data do very strongly prefer the presence of a gamma-ray component with a morphology similar to that predicted from annihilating dark matter (see Appendices B and D for further details).[2]

As in Ref. [8], we vary the value of the inner slope of the generalized NFW profile, γ, and compare the change in the log-likelihood, $\Delta \ln \mathcal{L}$, between the resulting fits in order to determine the preferred range for the value of γ.[3] The results of this exercise (as performed over 0.5-10 GeV) are shown in the left frame of Fig. 5. While previous fits (which did not employ any additional cuts on CTBCORE) preferred an inner slope of $\gamma \simeq 1.2$ [8], we find that a slightly steeper value of $\gamma \simeq 1.26$ provides the best fit to the data. Also, in contrast to Ref. [8], we find no significant difference in the slope preferred by the fit over the entire sky, and by a fit only over the southern sky ($b < 0$). This can be seen directly from the left frame of Fig. 5, where the full-sky and southern-sky fits for the same level of masking are found to favor quite similar values of γ (the southern sky distribution is broader than that for the full sky simply due to the difference in the number of photons).

In the right frame of Fig. 5, we show the spectrum of the emission correlated with the dark matter template, for the best-fit value of $\gamma = 1.26$. While no significant emission is absorbed by this template at energies above $\sim$10 GeV, a bright and robust component is present at lower energies, peaking near $\sim$1-3 GeV. Relative to the

[2] Previous studies [8, 9] have taken the approach of fitting for the spectrum of the *Fermi* Bubbles as a function of latitude, and then subtracting an estimated underlying spectrum for the Bubbles (based on high-latitude data) in order to extract the few-GeV excess. However, this approach discards information on the true morphology of the signal, as well as requiring an assumption for the Bubbles spectrum. It was shown in Ref. [8] (and also in this work, see Appendices B and D) that the excess is not confined to the Bubbles and the fit strongly prefers to correlate it with a dark matter template if one is available.

[3] Throughout, we denote the quantity $-2\ln\mathcal{L}$ by χ^2.

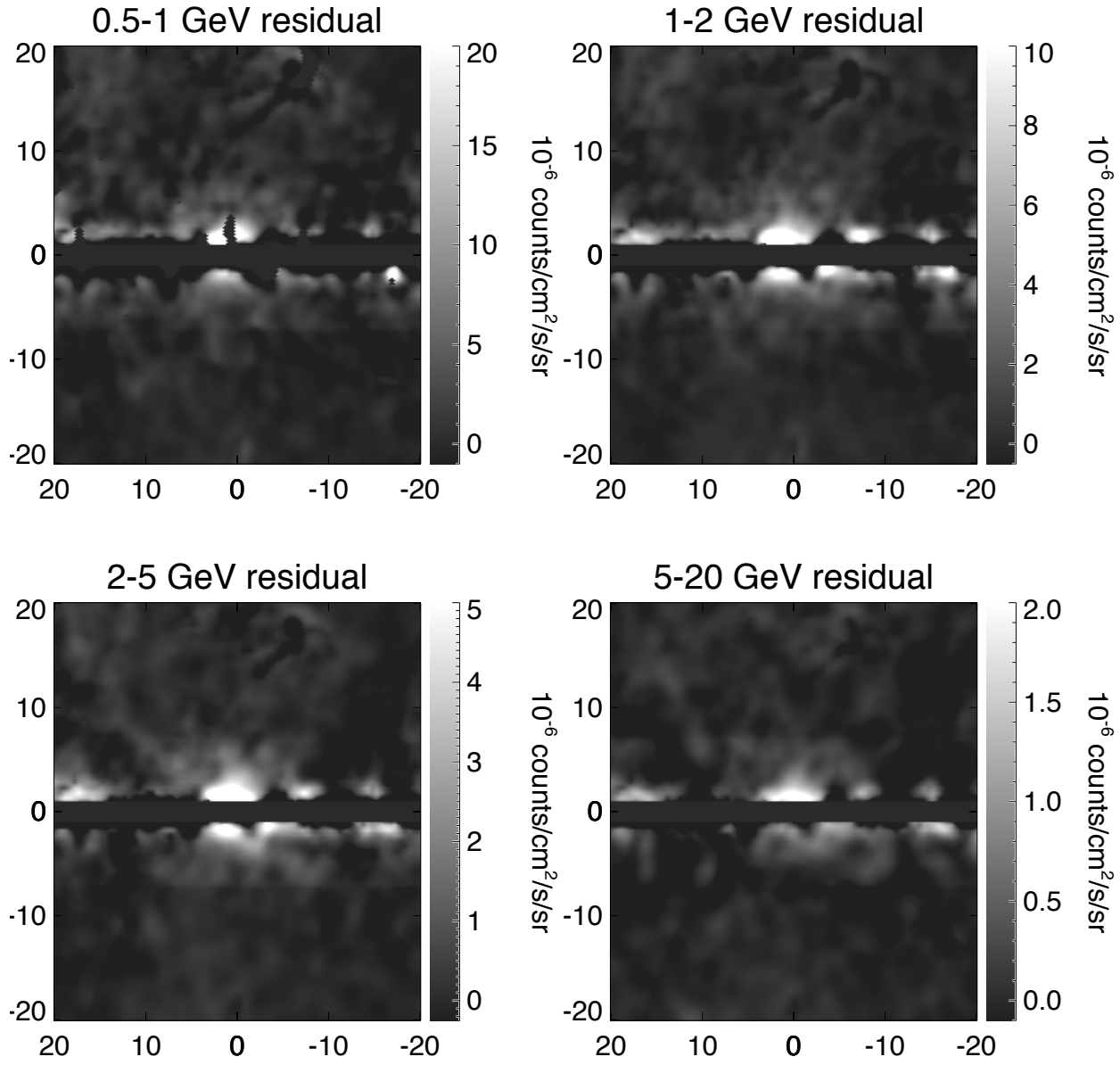

FIG. 6: Intensity maps (in galactic coordinates) after subtracting the best-fit Galactic diffuse model, *Fermi* bubbles, and isotropic templates. At energies between ∼0.5-5 GeV (*i.e.* in the first three frames), the dark-matter-like emission is clearly visible around the Galactic Center.

analysis of Ref. [8], the cut on CTBCORE significantly hardens the spectrum at energies below 1 GeV, rendering it more consistent with that extracted at higher latitudes (see Appendix A). Shown for comparison (as a solid line) is the spectrum predicted from a 35.25 GeV dark matter particle annihilating to $b\bar{b}$ with a cross section of $\sigma v = 1.7 \times 10^{-26}$ cm^3/s $\times [(0.3\,\mathrm{GeV/cm^3})/\rho_{\mathrm{local}}]^2$. The spectrum of this component is in good agreement with that predicted by this dark matter model, yielding a fit of $\chi^2 = 26.4$ over the 25 error bars between 0.3 and 100 GeV. We also note that the spectral shape of the dark matter template is quite robust to variations in γ, except at energies below $\sim$ 600 MeV, where the spectral shape can vary non-negligibly with the choice of inner slope (see Appendix C).

In Fig. 6, we plot the maps of the gamma-ray sky in four energy ranges after subtracting the best-fit diffuse model, *Fermi* Bubbles, and isotropic templates. In the 0.5-1 GeV, 1-2 GeV, and 2-5 GeV maps, the dark-matter-like emission is clearly visible in the region surrounding the Galactic Center. Much less central emission is visible at 5-20 GeV, where the dark matter component is significantly less bright.

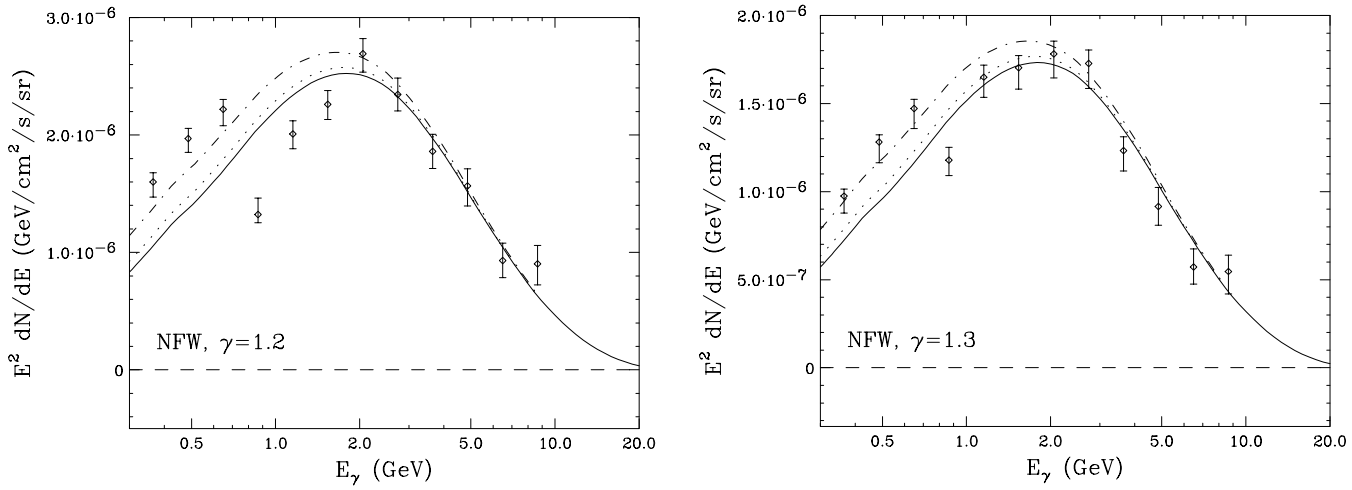

FIG. 7: The spectrum of the dark matter component derived in our Galactic Center analysis, for a template corresponding to an NFW halo profile with an inner slope of $\gamma = 1.2$ (left) or 1.3 (right), normalized to the flux at an angle of 5° from the Galactic Center. We caution that significant and difficult to estimate systematic uncertainties exist in this determination, especially at energies below ∼1 GeV. Shown for comparison (solid line) is the spectrum predicted from a 35.25 GeV dark matter particle annihilating to $b\bar{b}$ with a cross section of $\sigma v = 2.15 \times 10^{-26}$ cm^3/s $\times [(0.3\,\mathrm{GeV/cm^3})/\rho_{\mathrm{local}}]^2$ (left) or $\sigma v = 1.0 \times 10^{-26}$ cm^3/s $\times [(0.3\,\mathrm{GeV/cm^3})/\rho_{\mathrm{local}}]^2$ (right). The dot-dash and dotted curves include an estimated contribution from bremsstrahlung, as shown in the right frame of Fig. 2.

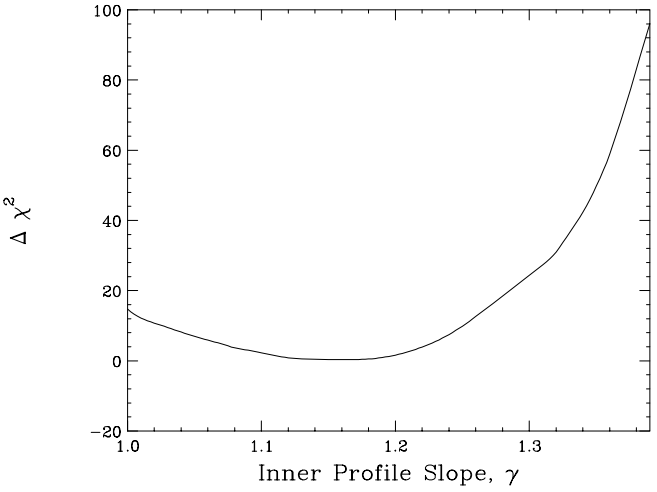

FIG. 8: The value of $\Delta\chi^2$ as a function of the inner slope of the dark matter halo profile, γ, as found in our Galactic Center likelihood analysis. The best-fit value is somewhat shallower than found in our analysis of the larger Inner Galaxy region, favoring $\gamma \sim 1.17$ (rather than $\gamma \simeq 1.26$).

V. THE GALACTIC CENTER

In this section, we describe our analysis of the *Fermi* data from the region of the Galactic Center, defined as $|b| < 5°$, $|l| < 5°$. We make use of the same Pass 7 data set, with Q2 cuts on CTBCORE, as described in the previous section. We performed a binned likelihood analysis to this data set using the *Fermi* tool `gtlike`, dividing the region into 200×200 spatial bins (each $0.05° \times 0.05°$), and 12 logarithmically-spaced energy bins between 0.316-10.0 GeV. Included in the fit is a model for the Galactic diffuse emission, supplemented by a model spatially tracing the observed 20 cm emission [43], a model for the isotropic gamma-ray background, and all gamma-ray sources listed in the 2FGL catalog [44], as well as the two additional point sources described in Ref. [45]. We allow the flux and spectral shape of all high-significance ($\sqrt{\mathrm{TS}} > 25$) 2FGL sources located within 7° of the Galactic Center to vary. For somewhat more distant or lower significance sources ($\psi = 7° - 8°$ and $\sqrt{\mathrm{TS}} > 25$, $\psi = 2° - 7°$ and $\sqrt{\mathrm{TS}} = 10 - 25$, or $\psi < 2°$ and any TS), we adopt the best-fit spectral shape as presented in the 2FGL catalog, but allow the overall normalization to float. We additionally allow the spectrum and normalization of the two new sources from Ref. [45], the 20 cm template, and the extended sources W28 and W30 [44] to float. We fix the emission from all other sources to the best-fit 2FGL values. For the Galactic diffuse emission, we adopt the model `gal_2yearp7v6_v0`. Although an updated Galactic diffuse model has recently been released by the *Fermi* Collaboration, that model includes additional empirically fitted features at scales greater than 2°, and therefore is not recommended for studies of extended gamma-ray emission. For the isotropic component, we adopt the model of Ref. [46]. We allow the overall normalization of the Galactic diffuse and isotropic emission to freely vary. In our fits, we found that the isotropic component prefers a normalization that is considerably brighter than the extragalactic gamma-ray background. In order to account for this additional isotropic emission in our region of interest, we attempted simulations in which we allowed the spectrum of the isotropic compo-

nent to vary, but found this to have a negligible impact on the fit.

In addition to these astrophysical components, we include a spatially extended model in our fits motivated by the possibility of annihilating dark matter. The morphology of this component is again taken to follow the line-of-sight integral of the square of the dark matter density, as described in Sec. II. We adopt a generalized NFW profile centered around the location of Sgr A* ($b = -0.04608^\circ$, $l = -0.05578^\circ$ [47]), and allow the inner slope (γ) and overall normalization (set by the annihilation cross section) to freely float.

In Figs. 7 and 8, we show the main results of our Galactic Center likelihood analysis. In Fig. 8, we plot the change of the log-likelihood of our fit as a function of the inner slope of the halo profile, γ. For our best-fit value of $\gamma = 1.17$, the inclusion of the dark matter component can improve the overall fit by $\Delta\chi^2 \simeq 300$, corresponding to a statical preference for such a component at the level of $\sim 17\sigma$. In Fig. 7, we show the spectrum of the dark-matter-like component, for values of $\gamma = 1.2$ (left frame) and $\gamma = 1.3$ (right frame). Shown for comparison is the spectrum predicted from a 35.25 GeV WIMP annihilating to $b\bar{b}$ (the same mass and annihilation channel as shown in Fig. 5). The solid line represents the contribution from prompt emission, whereas the dot-dashed and dotted lines also include an estimate for the contribution from bremsstrahlung (for the $z = 0.15$ and 0.3 kpc cases, as shown in the right frame of Fig. 2, respectively). The normalizations of the Galactic Center and Inner Galaxy signals are compatible (see Figs. 5 and 7), although the details of this comparison depend on the precise morphology that is adopted.

We note that the *Fermi* tool `gtlike` determines the quality of the fit assuming a given spectral shape for the dark matter template, but does not generally provide a model-independent spectrum for this or other components. In order to make a model-independent determination of the dark matter component's spectrum, we adopt the following procedure. First, assuming a seed spectrum for the dark matter component, the normalization and spectral shape of the various astrophysical components are each varied and set to their best-fit values. Then, the fit is performed again, allowing the spectrum of the dark matter component to vary in each energy bin. The resultant dark matter spectrum is then taken to be the new seed, and this procedure is repeated iteratively until convergence is reached.

In Fig. 9, we plot the gamma-ray count maps of the Galactic Center region. In the left frames, we show the raw maps, while in the right frames we have subtracted the best-fit contributions from each component in the fit except for that corresponding to the dark matter template (the Galactic diffuse model, 20 cm template, point sources, and isotropic template). In each frame, the map has been smoothed by a 0.25° Gaussian (0.59° full-width-half-maximum). The excess emission is clearly present in the right frames, and most evidently in the 1.0-3.16 GeV range, where the signal is most significant.

We note that the slope favored by our Galactic Center analysis ($\gamma \simeq 1.04$–1.24) is somewhat shallower than that found in Inner Galaxy analysis ($\gamma \simeq 1.26$). While this may arise from a systematic issue related to the spatial morphology of our diffuse templates, it is also plausible that the dark matter slope could vary with distance from the Galactic Center, for example as exhibited by an Einasto profile [32]. This could reconcile our results with those of the recent analysis of Ref. [7], which studied a smaller region of the sky ($|b| < 3.5^\circ$, $|l| < 3.5^\circ$) than our analyses, and found a preference for a somewhat shallower profile slope, $\gamma \simeq 1.12 \pm 0.05$.

As mentioned above, in addition to the Galactic diffuse model, we include a spatial template in our fit with a morphology tracing the 20 cm (1.5 GHz) map of Ref. [43]. This map is dominated by synchrotron emission, and thus traces a convolution of the distribution of cosmic-ray electrons and magnetic fields in the region. As cosmic-ray electrons also generate gamma rays via bremsstrahlung and inverse Compton processes, the inclusion of the 20 cm template in our fit is intended to better account for these sources of gamma rays. And although the Galactic diffuse model already includes contributions from bremsstrahlung and inverse Compton emission, the inclusion of this additional template allows for more flexibility in the fit. In actuality, however, we find that this template has only a marginal impact on the results of our fit, absorbing some of the low energy emission that (without the 20 cm template) would have been associated with our dark matter template.

VI. FURTHER CONSTRAINING THE MORPHOLOGY OF THE ANOMALOUS GAMMA-RAY EMISSION

In the previous two sections, we showed that the gamma-ray emission observed from the regions of the Inner Galaxy and Galactic Center is significantly better fit when we include an additional component with an angular distribution that follows that predicted from annihilating dark matter. In particular, our fits favor a morphology for this component that follows the square of a generalized NFW halo profile with an inner slope of $\gamma \simeq 1.1 - 1.3$. Implicit in those fits, however, was the assumption that the angular distribution of the anomalous emission is spherically symmetric with respect to the dynamical center of the Milky Way. In this section, we challenge this assumption and test whether other morphologies might provide a better fit to the observed emission.

We begin by considering templates which are elongated either along or perpendicular to the direction of the Galactic Plane. In Fig. 10, we plot the $\Delta\chi^2$ of the Inner Galaxy (left) and Galactic Center (right) fits with such an asymmetric template. The axis ratio is defined such that values less than unity are elongated in the direction

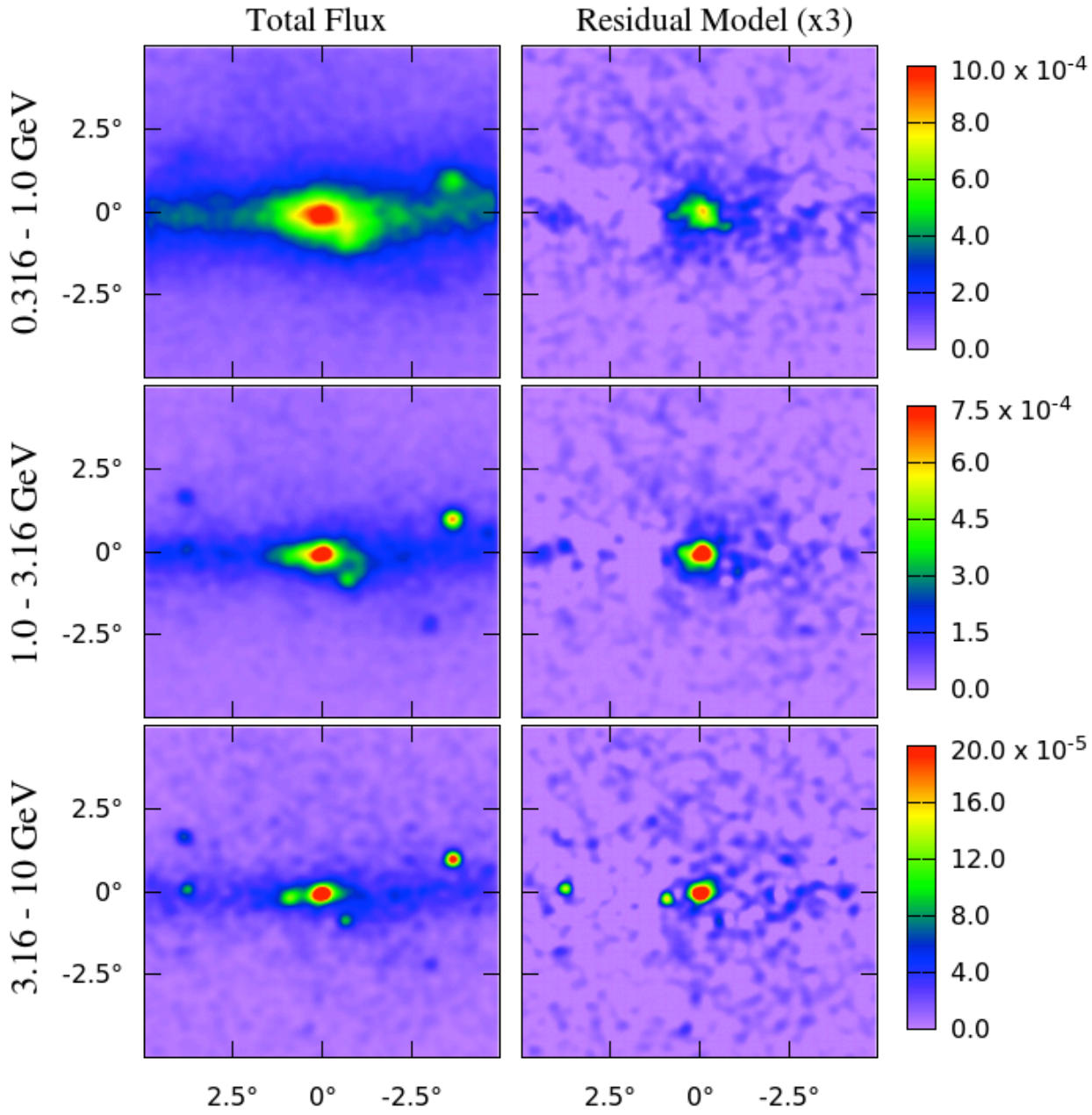

FIG. 9: The raw gamma-ray maps (left) and the residual maps after subtracting the best-fit Galactic diffuse model, 20 cm template, point sources, and isotropic template (right), in units of photons/cm^2/s/sr. The right frames clearly contain a significant central and spatially extended excess, peaking at ∼1-3 GeV. Results are shown in galactic coordinates, and all maps have been smoothed by a 0.25° Gaussian.

of the Galactic Plane, while values greater than one are preferentially extended perpendicular to the plane. In each case, the profile slope averaged over all orientations is taken to be $\gamma = 1.3$ (left) and 1.2 (right). From this figure, it is clear that the gamma-ray excess prefers to be fit by an approximately spherically symmetric distribution, and disfavors any axis ratio which departs from unity by more than approximately 20%.

In Fig. 11, we generalize this approach within our Galactic Center analysis to test morphologies that are not only elongated along or perpendicular to the Galactic Plane, but along any arbitrary orientation. Again, we find that that the quality of the fit worsens if the the template is significantly elongated either along or perpendicular to the direction of the Galactic Plane. A mild statistical preference is found, however, for a morphology with an axis ratio of ∼1.3-1.4 elongated along an axis rotated ∼35° counterclockwise from the Galactic Plane in galactic coordinates (a similar preference was also found in our Inner Galaxy analysis). While this may be a statis-

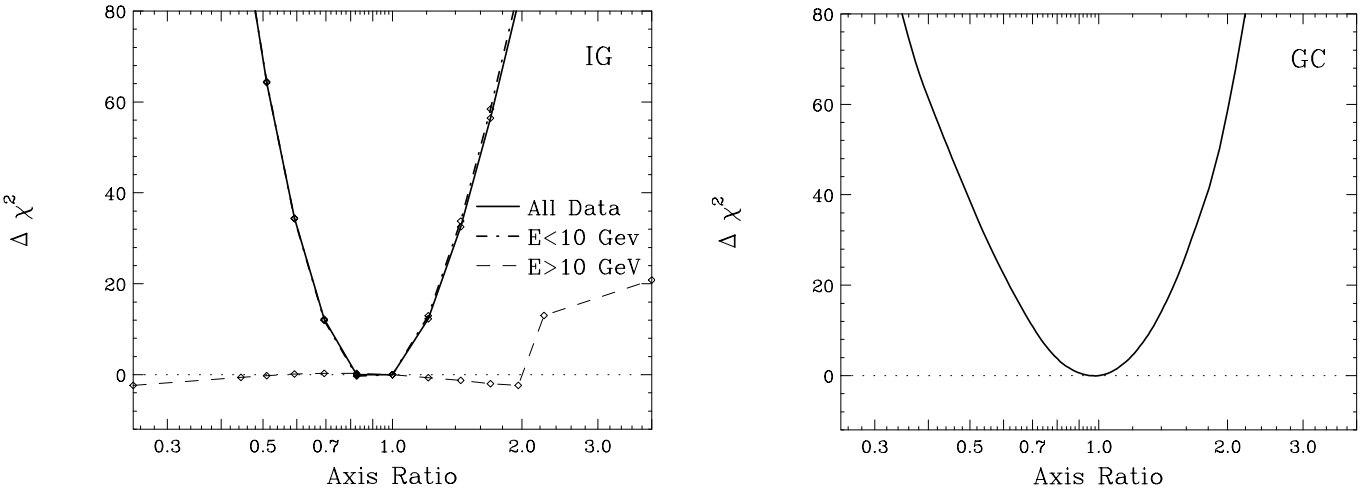

FIG. 10: The change in the quality of the fit, as performed in Sec. IV's Inner Galaxy analysis (left frame) and Sec. V's Galactic Center analysis (right frame), when breaking our assumption of spherical symmetry for the dark matter template. The axis ratio is defined such that values less than one are elongated along the Galactic Plane, whereas values greater than one are elongated with Galactic latitude. The fit strongly prefers a morphology for the anomalous component that is approximately spherically symmetric, with an axis ratio near unity.

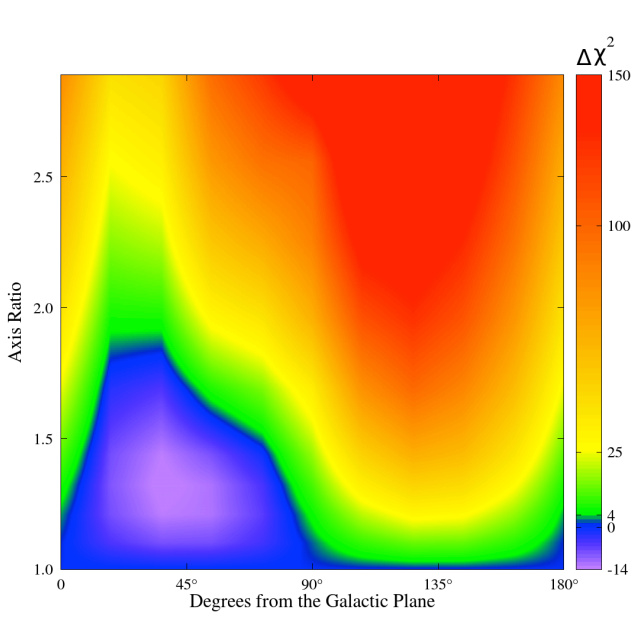

FIG. 11: The change in the quality of the fit in our Galactic Center analysis, for a dark matter template that is elongated along an arbitrary orientation (x-axis) and with an arbitrary axis ratio (y-axis). As shown in Fig. 10, the fit worsens if the this template is significantly stretched either along or perpendicular to the direction of the Galactic Plane (corresponding to 0° or 90° on the x-axis, respectively). A mild statistical preference, however, is found for a morphology with an axis ratio of ∼1.3-1.4 elongated along an axis rotated ∼35° counterclockwise from the Galactic Plane.

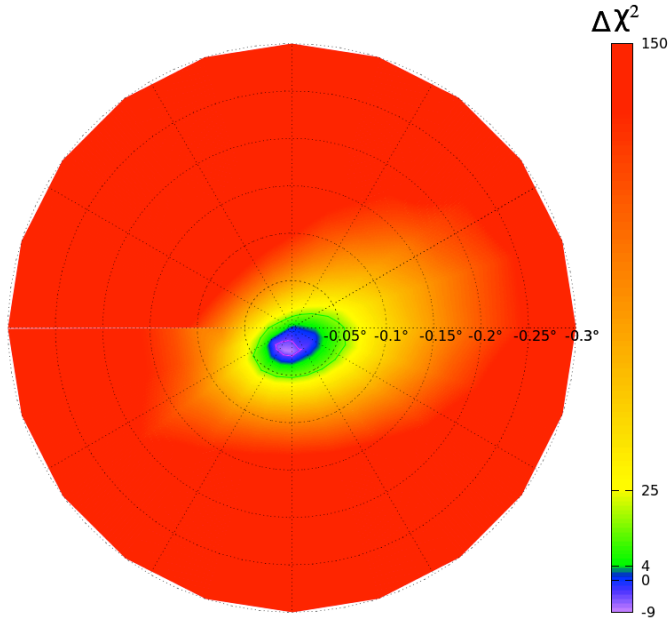

FIG. 12: To test whether the excess emission is centered around the dynamical center of the Milky Way (Sgr A*), we plot the $\Delta\chi^2$ of the fit found in our Galactic Center analysis, as a function of the center of our dark matter template. The fit clearly prefers this template to be centered within ∼0.05° degrees of the location of Sgr A*.

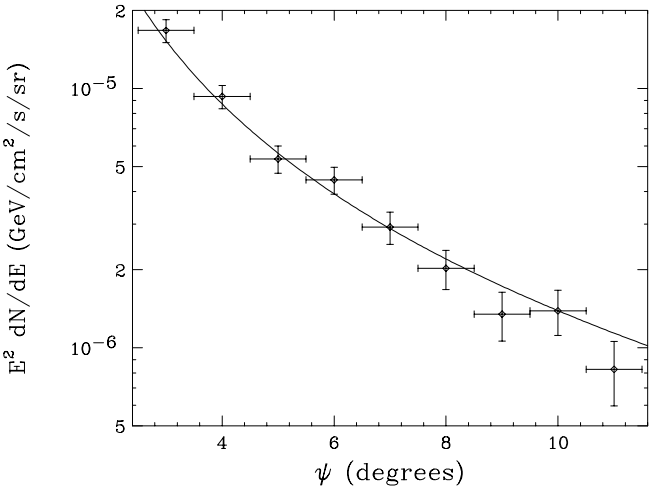

FIG. 13: To constrain the degree to which the gamma-ray excess is spatially extended, we have repeated our Inner Galaxy analysis, replacing the dark matter template with a series of concentric ring templates centered around the Galactic Center. The dark-matter-like emission is clearly and consistently present in each ring template out to $\sim$12°, beyond which systematic and statistical limitations make such determinations difficult. For comparison, we also show the predictions for a generalized NFW profile with $\gamma = 1.4$.

tical fluctuation, or the product of imperfect background templates, it could also potentially reflect a degree of triaxiality in the underlying dark matter distribution.

We have also tested whether the excess emission is, in fact, centered around the dynamical center of the Milky Way (Sgr A*), as we have thus far assumed. In Fig. 12, we plot the $\Delta\chi^2$ of the fit found in our Galactic Center analysis, as a function of the center of our dark matter-motivated template. The fit clearly prefers this template to be centered within $\sim$0.05° degrees of the location of Sgr A*.

An important question to address is to what degree the gamma-ray excess is spatially extended, and over what range of angles from the Galactic Center can it be detected? To address this issue, we have repeated our Inner Galaxy analysis, replacing the dark matter template with a series of concentric ring templates, each 1° wide, and centered around the Galactic Center. We smooth the ring templates to a 1° Gaussian (full-width-half-max), and fit the normalization of each ring template independently. Instead of allowing the spectrum of the ring templates to each vary freely (which would have introduced an untenable number of free parameters), we fix their spectral shape to that found for the dark matter component in the single template fit. We also break the template associated with the *Fermi* Bubbles into five templates, in 10° latitude slices (each with the same spectrum, but with independent normalizations).

The results of this fit are shown in Fig. 13. The dark-matter-like emission is clearly and consistently present in each ring template out to $\sim$12°, beyond which systematic and statistical limitations make such determinations difficult. For comparison, we also show the predictions for a generalized NFW profile with $\gamma = 1.4$ (after appropriate smoothing). While this value for the profile slope is slightly steeper that that found in Secs IV and V, we caution that systematic uncertainties associated with the diffuse model template may be biasing this fit toward somewhat steeper values of γ. This is consistent with results from the inner Galaxy analysis when the Galactic plane is masked at 2 degrees, which also suggest a slightly steeper profile slope.

To address the same question within the context of our Galactic Center analysis, we have re-performed our fit using dark matter templates which are based on density profiles which are set to zero beyond a given radius. We find that templates corresponding to density profiles set to zero outside of 800 pc (600 pc, 400 pc) provide a fit that is worse relative to that found using an untruncated template at the level of $\Delta\chi^2$=10.7 (57.6,108, respectively).

We have also tested our Galactic Center fit to see if a cored dark matter profile could also provide a good fit to the data. We find, however, that the inclusion of even a fairly small core is disfavored. Marginalizing over the inner slope of the dark matter profile, we find that flattening the density profile within a radius of 10 pc (30 pc, 50 pc, 70 pc, 90 pc) worsens the overall fit by $\Delta\chi^2$=3.6 (12.2, 22.4, 30.6, 39.2, respectively). The fit thus strongly disfavors any dark matter profile with a core larger than a few tens of parsecs.

Lastly, we confirm that the morphology of the anomalous emission does not significantly vary with energy. If we fit the inner slope of the dark matter template in our Inner Galaxy analysis one energy bin at a time, we find a similar value of $\gamma \sim$1.2-1.3 for all bins between 0.5 and 10 GeV. At energies below 0.5 GeV, the fit prefers somewhat steeper slopes ($\gamma \sim 1.6$) and a corresponding spectrum with a very soft spectral index, probably reflecting contamination from the Galactic Plane. At energies above 10 GeV, the fit prefers a lower value for the inner slope ($\gamma \sim 1.0$), suggesting that the residual emission found above 10 GeV is most likely associated with other residual structures, and not with the steepened NFW-like profile consistently preferred in the 0.5-10 GeV range.

The results described in this section indicate that the gamma-ray excess exhibits a morphology which is both approximately spherically symmetric and steeply falling (yet detectable) over two orders of magnitude in galactocentric distance (between $\sim$20 pc and $\sim$2 kpc from Sgr A*). This result is to be expected if the emission is produced by annihilating dark matter particles, but is not anticipated for any proposed astrophysical mechanisms or sources of this emission.

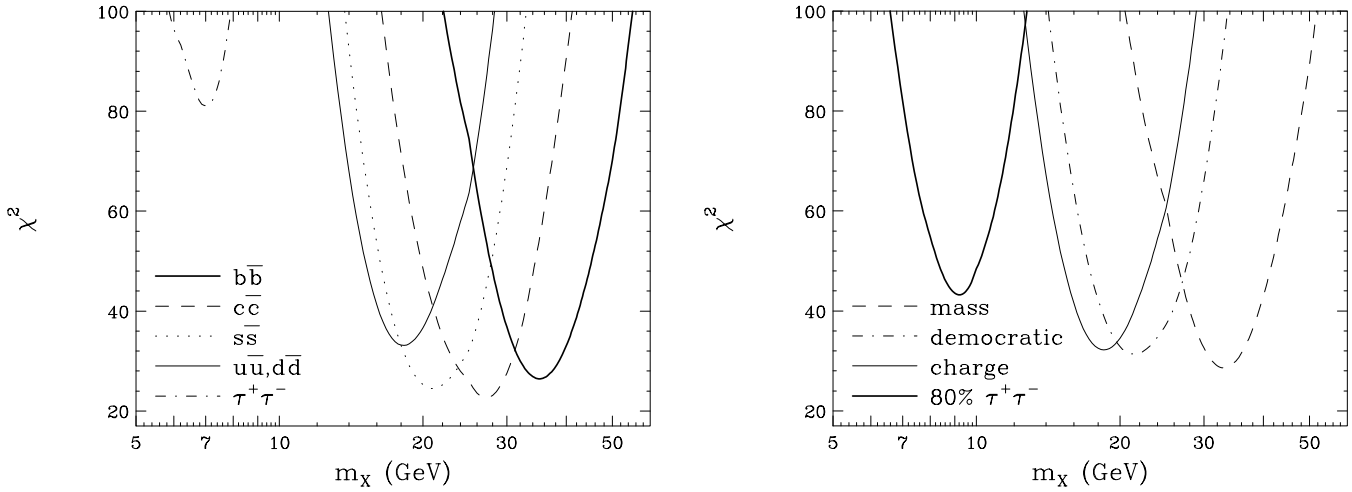

FIG. 14: The quality of the fit (χ^2, over 25-1 degrees-of-freedom) for various annihilating dark matter models to the spectrum of the anomalous gamma-ray emission from the Inner Galaxy (as shown in Fig. 5) as a function of mass, and marginalized over the value of the annihilation cross section. In the left frame, we show results for dark matter particles which annihilate uniquely to $b\bar{b}$, $c\bar{c}$, $s\bar{s}$, light quarks ($u\bar{u}$ and/or $d\bar{d}$), or $\tau^+\tau^-$. In the right frame, we consider models in which the dark matter annihilates to a combination of channels, with cross sections proportional to the square of the mass of the final state particles, the square of the charge of the final state particles, democratically to all kinematically accessible Standard Model fermions, or 80% to $\tau^+\tau^-$ and 20% to $b\bar{b}$. The best fits are found for dark matter particles with masses in the range of ∼20-40 GeV and which annihilate mostly to quarks.

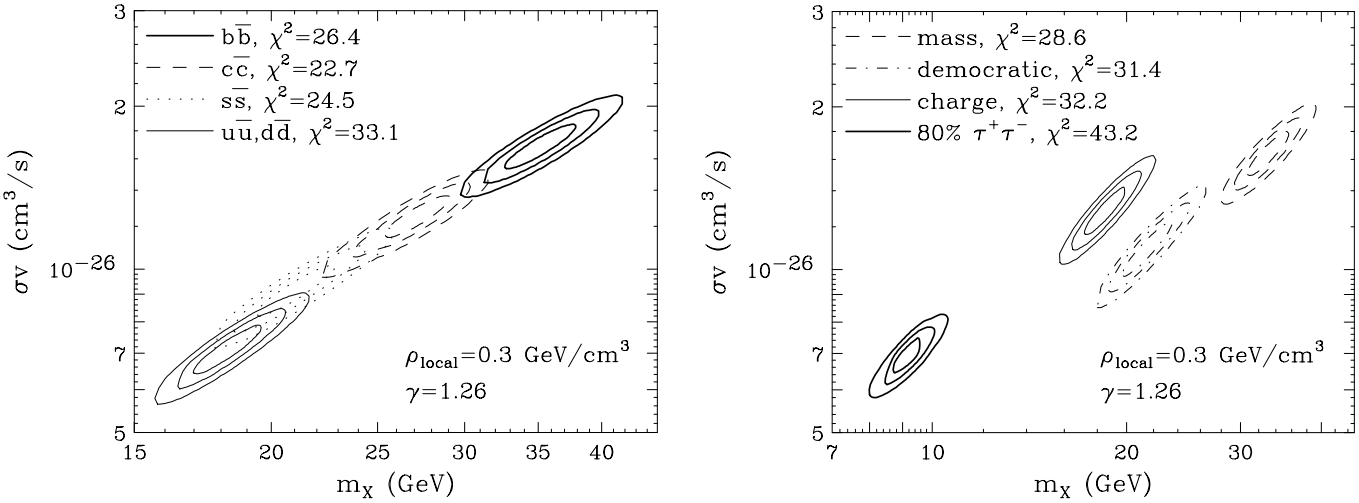

FIG. 15: The range of the dark matter mass and annihilation cross section required to fit the gamma-ray spectrum observed from the Inner Galaxy, for a variety of annihilation channels or combination of channels (see Fig. 14). The observed gamma-ray spectrum is generally best fit by dark matter particles with a mass of ∼20-40 GeV and that annihilate to quarks with a cross section of $\sigma v \sim (1-2) \times 10^{-26}$ cm^3/s.

VII. IMPLICATIONS FOR DARK MATTER

In this section, we use the results of the previous sections to constrain the characteristics of the dark matter particle species potentially responsible for the observed gamma-ray excess. We begin by fitting various dark matter models to the spectrum of the gamma-ray excess as found in our Inner Galaxy analysis (as shown in Fig. 5). In Fig. 14, we plot the quality of this fit (χ^2) as a function of the WIMP mass, for a number of dark matter annihilation channels (or combination of channels), marginalized over the value of the annihilation cross section. Given that this fit is performed over 25-1 degrees-of-freedom, a goodness-of-fit with a p-value of 0.05 (95% CL) corresponds to a χ^2 of approximately 36.8. We take any value less than this to constitute a "good fit" to the Inner Galaxy spectrum. Excellent fits are found for dark matter that annihilates to bottom, strange, or charm quarks

(χ^2 = 26.4, 24.5, and 22.7, respectively), and good fits are found for annihilations to light quarks, or to combinations of fermions proportional to the square of the mass of the final state, the square of the charge of the final state, or equally to all fermonic degrees of freedom (democratic). In the light mass region (m_X∼7-10 GeV) motivated by various direct detection anomalies [48–53], the best fit we find is for annihilations which proceed mostly to $\tau^+\tau^-$, with an additional small fraction to quarks, such as $b\bar{b}$. Even this scenario, however, provides a somewhat poor fit, significantly worse that that found for heavier ($m_X \sim 20 - 40$ GeV) dark matter particles annihilating mostly to quarks.

In Fig. 15, we show the regions of the dark matter mass-annihilation cross section plane that are best fit by the gamma-ray spectrum shown in Fig. 5. For each annihilation channel (or combination of channels), the 1, 2 and 3σ contours are shown around the best-fit point (corresponding to $\Delta\chi^2$ = 2.30, 6.18, and 11.83, respectively). Again, in the left frame we show results for dark matter particles which annihilate entirely to a single final state, while the right frame considers instead combinations of final states. Generally speaking, the best-fit models are those in which the dark matter annihilates to second or third generation quarks with a cross section of $\sigma v \sim (1-2) \times 10^{-26}$ cm^3/s.[4]

This range of values favored for the dark matter's annihilation cross section is quite interesting from the perspective of early universe cosmology. For the mass range being considered here, a WIMP with an annihilation cross section of $\sigma v \simeq 2.2 \times 10^{-26}$ cm^3/s (as evaluated at the temperature of freeze-out) will freeze-out in the early universe with a relic abundance equal to the measured cosmological dark matter density (assuming the standard thermal history) [54]. The dark matter annihilation cross section evaluated in the low-velocity limit (as is relevant for indirect searches), however, is slightly lower than the value at freeze-out in many models. For a generic s-wave annihilation process, for example, one generally expects dark matter in the form of a thermal relic to annihilate at low-velocities with a cross section near $\sigma v_{v=0} \simeq (1-2) \times 10^{-26}$ cm^3/s, in good agreement with the range of values favored by the observed gamma-ray excess.

Thus far in this section, we have fit the predictions of various dark matter models to the gamma-ray spectrum derived from our Inner Galaxy analysis. In Fig. 16, we compare the mass range best fit to the Inner Galaxy spectrum to that favored by our Galactic Center analysis. Overall, these two analyses favor a similar range of dark matter masses and annihilation channels, although the Galactic Center spectrum does appear to be slightly softer, and thus prefers WIMP masses that are a few GeV lower than favored by the Inner Galaxy analysis. This could, however, be the result of bremsstrahlung, which can soften the gamma-ray spectrum from dark matter in regions near the Galactic Plane (see Fig. 7 and the right frame of Fig. 2). Such emission could plausibly cause a 35 GeV WIMP, for example, to produce a gamma-ray spectrum along the Galactic Plane that resembles the prompt emission predicted from a ∼30-34 GeV WIMP.

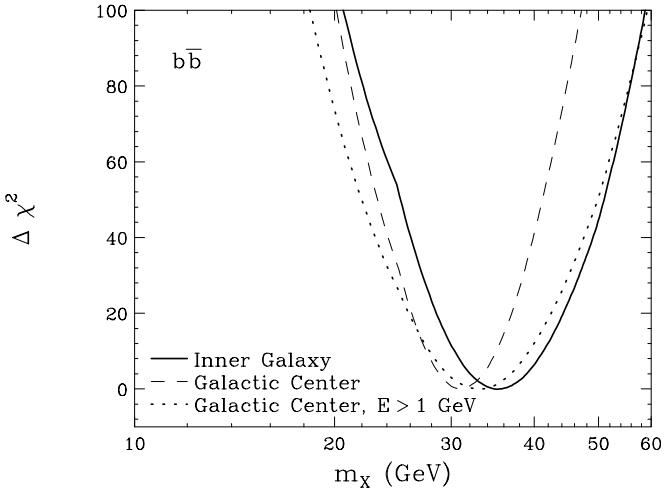

FIG. 16: A comparison of the dark matter mass determination using the spectrum derived from our Inner Galaxy analysis (solid line) and using the spectrum derived from our Galactic Center analysis (dashed and dotted lines). For each case shown, we have considered a profile with an inner slope of γ =1.3 and annihilations to $b\bar{b}$.

VIII. DISCUSSION

In this paper (and in previous studies [1, 2, 4–9]), it has been shown that the gamma-ray excess observed from the Inner Galaxy and Galactic Center is compatible with that anticipated from annihilating dark matter particles. This is not, however, the first time that an observational anomaly has been attributed to dark matter. Signals observed by numerous experiments, including *INTEGRAL* [55], *PAMELA* [56], *ATIC* [57], *Fermi* [58, 59], *WMAP* [60, 61], *DAMA/LIBRA* [52, 53], *CoGeNT* [48, 49], *CDMS* [50], and *CRESST* [51], among others, have received a great deal of attention as possible detections of dark matter particles. Most, if not all, of these signals, have nothing to do with dark matter, but instead result from some combination of astrophysical, environmental, and instrumental backgrounds. Given the frequency of such false alarms, we would be wise to apply a very high standard before concluding that

[4] The cross sections shown in Fig. 15 were normalized assuming a local dark matter density of 0.3 GeV/cm^3. Although this value is near the center of the range preferred by the combination of dynamical and microlensing data (for $\gamma = 1.26$), there are non-negligible uncertainties in this quantity. The analysis of Ref. [17], for example, finds a range of $\rho_{\rm local} = 0.24 - 0.46$ GeV/cm^3 at the 2σ level. This range of densities corresponds to a potential rescaling of the y-axis of Fig. 15 by up to a factor of 0.42-1.6.

any new signal is, in fact, the result of annihilating dark matter.

There are significant reasons to conclude, however, that the gamma-ray signal described in this paper is far more likely to be a detection of dark matter than any of the previously reported anomalies. Firstly, this signal consists of a very large number of events, and has been detected with overwhelming statistical significance. The the excess consists of $\sim 10^4$ gamma rays per square meter, per year above 1 GeV (from within 10° of the Galactic Center). Not only does this large number of events enable us to conclude with confidence that the signal is present, but it also allows us to determine its spectrum and morphology in some detail. And as shown, the measured spectrum, angular distribution, and normalization of this emission does indeed match well with that expected from annihilating dark matter particles.

Secondly, the gamma-ray signal from annihilating dark matter can be calculated straightforwardly, and generally depends on only a few unknown parameters. The morphology of this signal, in particular, depends only on the distribution of dark matter in the Inner Galaxy (as parameterized in our study by the inner slope, γ). The spectral shape of the signal depends only on the mass of the dark matter particle and on what Standard Model particles are produced in its annihilations. The Galactic gamma-ray signal from dark matter can thus be predicted relatively simply, in contrast to, *e.g.*, dark matter searches using cosmic rays, where putative signals are affected by poorly constrained diffusion and energy-loss processes. In other words, for the gamma-ray signal at hand, there are relatively few "knobs to turn", making it less likely that one would be able to mistakenly fit a well-measured astrophysical signal with an annihilating dark matter model.

Thirdly, we once again note that the signal described in this study can be explained by a very simple dark matter candidate, without any baroque or otherwise unexpected features. After accounting for uncertainties in the overall mass of the Milky Way's dark matter halo profile [17], our results favor dark matter particles with an annihilation cross section of $\sigma v = (0.7 - 3.9) \times 10^{-26}$ cm^3/s (for annihilations to $b\bar{b}$, see Fig. 15). This range covers the long predicted value that is required of a thermal relic that freezes-out in the early universe with an abundance equal to the measured cosmological dark matter density (2.2×10^{-26} cm^3/s). No substructure boost factors, Sommerfeld enhancements, or non-thermal histories are required. Furthermore, it is not difficult to construct simple models in which a $\sim$30-40 GeV particle annihilates to quarks with the required cross section without violating constraints from direct detection experiments, colliders, or other indirect searches (for work related to particle physics models capable of accommodating this signal, see Refs. [62–74]).

And lastly, the dark matter interpretation of this signal is strengthened by the absence of plausible or well motivated alternatives. There is no reason to expect that any diffuse astrophysical emission processes would exhibit either the spectrum or the morphology of the observed signal. In particular, the spherical symmetry of the observed emission with respect to the Galactic Center does not trace any combination of astrophysical components (*i.e.* radiation, gas, dust, star formation, etc.), but does follow the square of the anticipated dark matter density.

The astrophysical interpretation most often discussed within the context of this signal is that it might originate from a large population of unresolved millisecond pulsars. The millisecond pulsars observed within the Milky Way are largely located either within globular clusters or in or around the Galactic Disk (with an exponential scale height of $z_s \sim 1$ kpc [11, 75]). This pulsar population would lead to a diffuse gamma-ray signal that is highly elongated along the disk, and would be highly incompatible with the constraints described in Sec. VI. For example, the best-fit model of Ref. [75], which is based on the population of presently resolved gamma-ray millisecond pulsars, predicts a morphology for the diffuse gamma-ray emission exhibiting an axis ratio of $\sim$1-to-6. Within 10° of the Galactic Center, this model predicts that millisecond pulsars should account for $\sim$1% of the observed diffuse emission, and less than $\sim$5-10% of the signal described in this paper.

To evade this conclusion, however, one could contemplate an additional (and less constrained) millisecond pulsar population associated with the Milky Way's central stellar cluster. This scenario can be motivated by the fact that globular clusters are known to contain large numbers of millisecond pulsars, presumably as a consequence of their very high stellar densities. If our galaxy's central stellar cluster contains a large number of millisecond pulsars with an extremely concentrated distribution (with a number density that scales approximately as $n_{\rm MSP} \propto r^{-2.4}$), those sources could plausibly account for much of the gamma-ray excess observed within the inner $\sim 1^\circ$ around the Galactic Center [2, 4–7, 10]. It is much more challenging, however, to imagine that millisecond pulsars could account for the more extended component of this excess, which we have shown to be present out to at least $\sim 10^\circ$ from the Galactic Center. Expectations for the Inner Galaxy's pulsar population are not consistent with such an extended distribution. Furthermore, if the required number of millisecond pulsars were present $\sim 10^\circ$ ($\sim$1.5 kpc) north or south of the Galactic Center, a significant number of these sources would have been resolved by *Fermi* and appeared within the 2FGL catalog (assuming that the pulsars in question have a similar luminosity function to other observed millisecond pulsars) [11, 44, 75]. The lack of such resolved sources strongly limits the abundance of millisecond pulsars in the region of the Inner Galaxy. Furthermore, the shape of the gamma-ray spectrum observed from resolved millisecond pulsars and from globular clusters (whose emission is believed to be dominated by millisecond pulsars) appears to be not-insignificantly softer than that of the gamma-ray excess observed from the Inner Galaxy. In

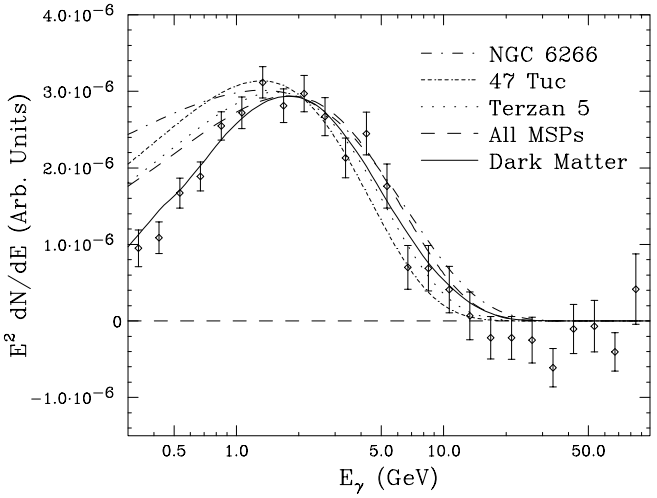

FIG. 17: A comparison of the spectral shape of the gamma-ray excess described in this paper (error bars) to that measured from a number of high-significance globular clusters (NGC 6266, 47 Tuc, and Terzan 5), and from the sum of all millisecond pulsars detected as individual point sources by *Fermi*. The gamma-ray spectrum measured from millisecond pulsars and from globular clusters (whose emission is believed to be dominated by millisecond pulsars) is consistently softer than that of the observed excess at energies below ∼1 GeV. See text for details.

Fig. 17, we compare the spectral shape of the gamma-ray excess to that measured from a number of globular clusters, and from the sum of all resolved millisecond pulsars. Here, we have selected the three highest significance globular clusters (NGC 6266, 47 Tuc, and Terzan 5), and plotted their best fit spectra as reported by the *Fermi* Collaboration [76]. For the emission from resolved millisecond pulsars, we include the 37 sources as described in Ref. [11]. Although each of these spectral shapes provides a reasonably good fit to the high-energy spectrum, they also each significantly exceed the amount of emission that is observed at energies below ∼1 GeV. This comparison further disfavors millisecond pulsars as the source of the observed gamma-ray excess.

The near future offers encouraging prospects for detecting further evidence in support of a dark matter interpretation of this signal. The dark matter mass and annihilation cross section implied by the gamma-ray excess is similar to *Fermi*'s sensitivity from observations of dwarf spheroidal galaxies. In fact, the *Fermi* Collaboration has reported a modestly statistically significant excess (∼2-3σ) in their search for annihilating dark matter particles in dwarf galaxies. If interpreted as a detection of dark matter, this observation would imply a similar mass and cross section to that favored by our analysis [33]. A similar (∼3σ) excess has also been reported from the direction of the Virgo Cluster [77, 78]. With the full dataset anticipated from *Fermi*'s 10 year mission, it may be possible to make statistically significant detections of dark matter annihilation products from a few of the brightest dwarf galaxies, galaxy clusters, and perhaps nearby dark matter subhalos [79]. Anticipated measurements of the cosmic-ray antiproton-to-proton ratio by *AMS* may also be sensitive to annihilating dark matter with the characteristics implied by our analysis [80, 81].

IX. SUMMARY AND CONCLUSIONS

In this study, we have revisited and scrutinized the gamma-ray emission from the central regions of the Milky Way, as measured by the *Fermi* Gamma-Ray Space Telescope. In doing so, we have confirmed a robust and highly statistically significant excess, with a spectrum and angular distribution that is in excellent agreement with that expected from annihilating dark matter. The signal is distributed with approximate spherical symmetry around the Galactic Center, with a flux that falls off as $F_\gamma \propto r^{-(2.2-2.6)}$, implying a dark matter distribution of $\rho \propto r^{-\gamma}$, with $\gamma \simeq 1.1-1.3$. The spectrum of the excess peaks at ∼1-3 GeV, and is well fit by 31-40 GeV dark matter particles annihilating to $b\bar{b}$. The annihilation cross section required to normalize this signal is $\sigma v = (1.4-2.0) \times 10^{-26}$ cm^3/s (for a local dark matter density of 0.3 GeV/cm^3), in good agreement with the value predicted for a simple thermal relic. In particular, a dark matter particle with this cross section will freeze-out of thermal equilibrium in the early universe to yield an abundance approximately equal to the measured cosmological dark matter density (for the range of masses and cross sections favored for other annihilation channels, see Sec. VII).

In addition to carrying out two different analyses (as described in Secs. IV and V), subject to different systematic uncertainties, we have applied a number of tests to our results in order to more stringently determine whether the characteristics of the observed excess are in fact robust and consistent with the signal predicted from annihilating dark matter. These tests uniformly confirm that the signal is present throughout the Galactic Center and Inner Galaxy (extending out to angles of at least 10° from the Galactic Center), without discernible spectral variation or significant departures from spherical symmetry. No known, anticipated, or proposed astrophysical diffuse emission mechanisms can account for this excess. And while a population of several thousand millisecond pulsars could have plausibly been responsible for much of the anomalous emission observed from within the innermost $\sim 1^\circ - 2^\circ$ around the Galactic Center, the extension of this signal into regions well beyond the confines of the central stellar cluster strongly disfavors such objects as the primary source of this signal. In light of these considerations, we consider annihilating dark matter particles to be the leading explanation for the origin of this signal, with potentially profound implications for cosmology and particle physics.

Acknowledgements: We would like to thank Keith

Bechtol, Eric Charles and Alex Drlica-Wagner for their help with the Fermi-LAT likelihood analysis, Oscar Macias-Ramirez and Farhad Yusef-Zadeh for providing the 20 cm templates, and Jesse Thaler, Neal Weiner, and Simona Murgia for helpful discussions. We would also like to thank the *Fermi* Collaboration for providing the data used in this analysis. DPF is supported in part by the NASA Fermi Guest Investigator Program, DH is supported by the Department of Energy, and TL is supported by NASA through Einstein Postdoctoral Award Number PF3-140110. NLR is supported by the Arthur Kerman Fellowship. TRS is supported by the U.S. Department of Energy under cooperative research agreement Contract Number DE-FG02-05ER41360.

[1] L. Goodenough and D. Hooper (2009), 0910.2998.
[2] D. Hooper and L. Goodenough, Phys.Lett. **B697**, 412 (2011), 1010.2752.
[3] A. Boyarsky, D. Malyshev, and O. Ruchayskiy, Phys.Lett. **B705**, 165 (2011), 1012.5839.
[4] D. Hooper and T. Linden, Phys.Rev. **D84**, 123005 (2011), 1110.0006.
[5] K. N. Abazajian and M. Kaplinghat, Phys.Rev. **D86**, 083511 (2012), 1207.6047.
[6] C. Gordon and O. Macias, Phys.Rev. **D88**, 083521 (2013), 1306.5725.
[7] K. N. Abazajian, N. Canac, S. Horiuchi, and M. Kaplinghat (2014), 1402.4090.
[8] D. Hooper and T. R. Slatyer, Phys.Dark Univ. **2**, 118 (2013), 1302.6589.
[9] W.-C. Huang, A. Urbano, and W. Xue (2013), 1307.6862.
[10] K. N. Abazajian, JCAP **1103**, 010 (2011), 1011.4275.
[11] D. Hooper, I. Cholis, T. Linden, J. Siegal-Gaskins, and T. R. Slatyer, Phys.Rev. **D88**, 083009 (2013), 1305.0830.
[12] T. Linden, E. Lovegrove, and S. Profumo, Astrophys.J. **753**, 41 (2012), 1203.3539.
[13] O. Macias and C. Gordon (2013), 1312.6671.
[14] M. Kuhlen, J. Diemand, and P. Madau (2007), 0705.2037.
[15] J. F. Navarro, C. S. Frenk, and S. D. M. White, Astrophys. J. **462**, 563 (1996), astro-ph/9508025.
[16] J. F. Navarro, C. S. Frenk, and S. D. M. White, Astrophys. J. **490**, 493 (1997), astro-ph/9611107.
[17] F. Iocco, M. Pato, G. Bertone, and P. Jetzer, JCAP **1111**, 029 (2011), 1107.5810.
[18] R. Catena and P. Ullio (2009), 0907.0018.
[19] J. F. Navarro et al. (2008), 0810.1522.
[20] J. Diemand et al. (2008), arXiv: 0805.1244 [astro-ph].
[21] G. R. Blumenthal, S. M. Faber, R. Flores, and J. R. Primack, Astrophys. J. **301**, 27 (1986).
[22] B. S. Ryden and J. E. Gunn, Astrophys. J. **318**, 15 (1987).
[23] O. Y. Gnedin, D. Ceverino, N. Y. Gnedin, A. A. Klypin, A. V. Kravtsov, et al. (2011), 1108.5736.
[24] O. Y. Gnedin, A. V. Kravtsov, A. A. Klypin, and D. Nagai, Astrophys. J. **616**, 16 (2004), arXiv:astro-ph/0406247.
[25] F. Governato, A. Zolotov, A. Pontzen, C. Christensen, S. H. Oh, A. M. Brooks, T. Quinn, S. Shen, and J. Wadsley, Mon. Not. R. Astron. Soc. **422**, 1231 (2012), 1202.0554.
[26] M. Kuhlen, J. Guedes, A. Pillepich, P. Madau, and L. Mayer, Astrophys.J. **765**, 10 (2013), 1208.4844.
[27] M. D. Weinberg and N. Katz, Astrophys.J. **580**, 627 (2002), astro-ph/0110632.
[28] M. D. Weinberg and N. Katz, Mon.Not.Roy.Astron.Soc. **375**, 460 (2007), astro-ph/0601138.
[29] J. Sellwood, Astrophys.J. **587**, 638 (2003), astro-ph/0210079.
[30] O. Valenzuela and A. Klypin, Mon.Not.Roy.Astron.Soc. **345**, 406 (2003), astro-ph/0204028.
[31] P. Colin, O. Valenzuela, and A. Klypin, Astrophys.J. **644**, 687 (2006), astro-ph/0506627.
[32] V. Springel et al., Mon. Not. Roy. Astron. Soc. **391**, 1685 (2008), 0809.0898.
[33] M. Ackermann et al. (Fermi-LAT Collaboration) (2013), 1310.0828.
[34] T. Sjostrand, S. Mrenna, and P. Z. Skands, JHEP **0605**, 026 (2006), hep-ph/0603175.
[35] L. Bergstrom, T. Bringmann, M. Eriksson, and M. Gustafsson, Phys.Rev.Lett. **94**, 131301 (2005), astro-ph/0410359.
[36] A. Birkedal, K. T. Matchev, M. Perelstein, and A. Spray (2005), hep-ph/0507194.
[37] M. Cirelli, P. D. Serpico, and G. Zaharijas, JCAP **1311**, 035 (2013), 1307.7152.
[38] W. Atwood et al. (LAT Collaboration), Astrophys.J. **697**, 1071 (2009), 0902.1089.
[39] M. Ackermann et al. (Fermi-LAT Collaboration), Astrophys.J.Suppl. **203**, 4 (2012), 1206.1896.
[40] S. Portillo and D. Finkbeiner (in preparation) (2014).
[41] G. Dobler, D. P. Finkbeiner, I. Cholis, T. R. Slatyer, and N. Weiner, Astrophys.J. **717**, 825 (2010), 0910.4583.
[42] M. Su, T. R. Slatyer, and D. P. Finkbeiner, Astrophys.J. **724**, 1044 (2010), 1005.5480.
[43] C. Law, F. Yusef-Zadeh, W. Cotton, and R. Maddalena (2008), 0801.4294.
[44] P. Nolan et al. (Fermi-LAT Collaboration), Astrophys.J.Suppl. **199**, 31 (2012), 1108.1435.
[45] F. Yusef-Zadeh, J. Hewitt, M. Wardle, V. Tatischeff, D. Roberts, et al., Astrophys.J. **762**, 33 (2013), 1206.6882.
[46] A. Abdo et al. (Fermi-LAT collaboration), Phys. Rev. Lett. **104**, 101101 (2010), 1002.3603.
[47] F. Yusef-Zadeh, D. Choate, and W. Cotton, Astrophys. J. Lett. **518**, L33 (1999), astro-ph/9904142.
[48] C. Aalseth et al. (CoGeNT collaboration), Phys. Rev. Lett. **106**, 131301 (2011), 1002.4703.
[49] C. E. Aalseth et al. (2011), 1106.0650.
[50] R. Agnese et al. (CDMS Collaboration), Phys.Rev.Lett. (2013), 1304.4279.
[51] G. Angloher, M. Bauer, I. Bavykina, A. Bento, C. Bucci, et al., Eur.Phys.J. **C72**, 1971 (2012), 1109.0702.
[52] R. Bernabei et al. (DAMA), Eur. Phys. J. **C56**, 333 (2008), 0804.2741.
[53] R. Bernabei et al. (2010), 1002.1028.
[54] G. Steigman, B. Dasgupta, and J. F. Beacom, Phys.Rev. **D86**, 023506 (2012), 1204.3622.
[55] C. Boehm, D. Hooper, J. Silk, M. Casse, and J. Paul,

Phys. Rev. Lett. **92**, 101301 (2004), astro-ph/0309686.
[56] O. Adriani et al. (PAMELA), Nature **458**, 607 (2009), 0810.4995.
[57] J. Chang et al., Nature **456**, 362 (2008).
[58] C. Weniger, JCAP **1208**, 007 (2012), 1204.2797.
[59] M. Su and D. P. Finkbeiner (2012), 1206.1616.
[60] D. P. Finkbeiner (2004), astro-ph/0409027.
[61] D. Hooper, D. P. Finkbeiner, and G. Dobler, Phys. Rev. **D76**, 083012 (2007), arXiv:0705.3655 [astro-ph].
[62] C. Boehm, M. J. Dolan, C. McCabe, M. Spannowsky, and C. J. Wallace (2014), 1401.6458.
[63] K. P. Modak, D. Majumdar, and S. Rakshit (2013), 1312.7488.
[64] W.-C. Huang, A. Urbano, and W. Xue (2013), 1310.7609.
[65] N. Okada and O. Seto (2013), 1310.5991.
[66] K. Hagiwara, S. Mukhopadhyay, and J. Nakamura, Phys.Rev. **D89**, 015023 (2014), 1308.6738.
[67] M. R. Buckley, D. Hooper, and J. Kumar, Phys.Rev. **D88**, 063532 (2013), 1307.3561.
[68] L. A. Anchordoqui and B. J. Vlcek, Phys.Rev. **D88**, 043513 (2013), 1305.4625.
[69] M. R. Buckley, D. Hooper, and J. L. Rosner, Phys.Lett. **B703**, 343 (2011), 1106.3583.
[70] M. Boucenna and S. Profumo, Phys.Rev. **D84**, 055011 (2011), 1106.3368.
[71] G. Marshall and R. Primulando, JHEP **1105**, 026 (2011), 1102.0492.
[72] G. Zhu, Phys.Rev. **D83**, 076011 (2011), 1101.4387.
[73] M. R. Buckley, D. Hooper, and T. M. Tait, Phys.Lett. **B702**, 216 (2011), 1011.1499.
[74] H. E. Logan, Phys.Rev. **D83**, 035022 (2011), 1010.4214.
[75] T. Grgoire and J. Kndlseder (2013), 1305.1584.
[76] A. Abdo et al. (Fermi-LAT Collaboration) (2010), 1003.3588.
[77] J. Han, C. S. Frenk, V. R. Eke, L. Gao, S. D. White, et al., Mon.Not.Roy.Astron.Soc. **427**, 1651 (2012), 1207.6749.
[78] O. Macias-Ramirez, C. Gordon, A. M. Brown, and J. Adams, Phys.Rev. **D86**, 076004 (2012), 1207.6257.
[79] A. Berlin and D. Hooper, Phys.Rev. **D89**, 016014 (2014), 1309.0525.
[80] M. Cirelli and G. Giesen, JCAP **1304**, 015 (2013), 1301.7079.
[81] N. Fornengo, L. Maccione, and A. Vittino (2013), 1312.3579.
[82] D. J. Schlegel, D. P. Finkbeiner, and M. Davis, Astrophys. J. **500**, 525 (1998), astro-ph/9710327.

Appendix A: Spectral Variation and the Impact of Cuts on CTBCORE

The suppression of the tails of the point spread function (PSF) made possible by our cuts on the *Fermi* event parameter CTBCORE (as described in Sec. III) has had a pronounced effect on the results of our Inner Galaxy analysis. As noted above, the asymmetry previously found between the northern and southern sky [8] vanishes after applying this cut. Additionally, the preferred slope of the inner profile changes slightly, and the extracted spectral shape becomes much less dependent upon the value of this slope. More generally, the CTBCORE cut reduces the degree of variation found for the spectrum of the dark matter template when fitting over different regions. This is a noteworthy validation of the hypothesis that the excess has a single spectral shape, invariant over the sky.

In Fig. 18, we compare the spectrum correlated with the dark matter template (with $\gamma = 1.26$) for different degrees of masking the Galactic Plane ($|b| > 1^\circ$ and $|b| > 5^\circ$), and for fits performed over the entire sky or restricted to the southern sky (where the diffuse backgrounds are somewhat fainter). In the left frame, we show results for the dataset used throughout the bulk of this paper, including the application of cuts to CTBCORE. In the right frame, we compare this to the results found using the same dataset without any additional cuts on CTBCORE. We see that the CTBCORE cut substantially hardens the spectrum of the excess below 1 GeV for the $|b| > 1^\circ$ fits, bringing the spectral shapes found in different regions of the sky into much better agreement, as well as significantly reducing the north-south asymmetry that had been previously reported.

The discrepancy between the spectra observed in the absence of the CTBCORE cut most likely originates from the contamination of the $|b| > 1^\circ$ fits by diffuse emission from the Galactic Plane. Since the separation between templates is done using purely spatial information, long tails in the point spread function that are not adequately taken into account in the generation of the maps could potentially lead to the misattribution of photons between templates (or to the misattribution of photons from bright point sources to one of the templates). The brightest background template, especially near the Galactic Center, is that corresponding to the diffuse Galactic emission model. Even a relatively small fraction of these photons, if incorrectly attributed to the new component, can have a large impact on the spectrum of the extracted signal, especially at low energies where the excess correlated with the dark matter template is faint.

The spectrum of the Galactic diffuse emission does not vary dramatically over the Inner Galaxy, being largely determined by the spectrum of cosmic rays. If contamination by diffuse-background-correlated photons is responsible for the observed variation in the spectrum of the dark matter template, one might expect those misattributed photons to share a similar spectrum (although this is not *essential*, as the degree of misattribution could vary with energy). When studying the various spectra presented in Ref. [8], we find that this is indeed the case. A missubtraction (either over- or under-subtraction) of 5-10% of the diffuse background (in the region of the dark matter template, and weighted by that template) can entirely account for the differences between the spectra extracted for the dark matter template in different fits, in both shape and normalization. It is plausible that the disagreements in the literature over the spectral shape of the Galactic Center excess – for example, raising the question of whether it can be well fitted by $\sim$10 GeV

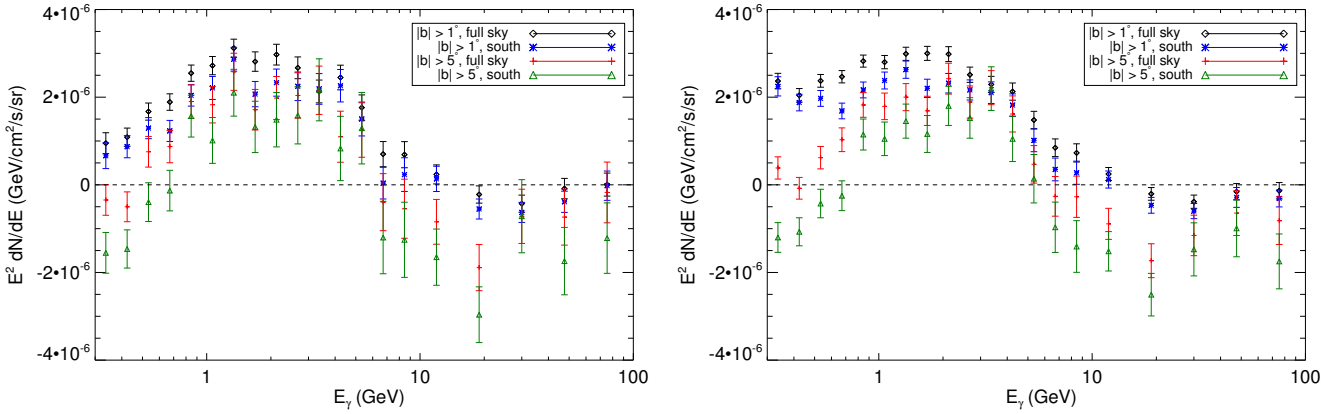

FIG. 18: The spectrum of the dark matter template found in our Inner Galaxy analysis when performing the fit over different regions of the sky ($|b| > 1^\circ$, $b < -1^\circ$, $|b| > 5^\circ$, and $b < -5^\circ$). All fits employ a single template for the Bubbles, the `p6v11` *Fermi* diffuse model, and a dark matter motivated signal template with an inner profile slope of $\gamma = 1.26$. In the left frame, we have applied our standard cuts on the *Fermi* event parameter CTBCORE (as described in Sec. III). In the right frame, no such additional cuts have been applied. The CTBCORE cut substantially hardens the spectrum of the excess below 1 GeV for the $|b| > 1^\circ$ fits, bringing the spectral shapes found in different regions of the sky into much better agreement, as well as significantly reducing the north-south asymmetry that had been previously reported.

dark matter annihilating to tau leptons, or by pulsars – can in large part be traced to the same uncertainties in the diffuse background modeling. The CTBCORE cut applied in this study, however, appears to have largely removed this contamination, at least in our analysis of the Inner Galaxy.

Appendix B: A Simple Test of Spherical Symmetry

Probing the morphology of the Inner Galaxy excess is complicated by the bright emission correlated with the Galactic Plane. In Ref. [8], it proved difficult to robustly determine whether any signal was present outside of the regions occupied by the *Fermi* Bubbles, as the regions both close to the Galactic Center and outside of the Bubbles were dominated by the bright emission from the Galactic Plane. The improvement in angular resolution resulting from our CTBCORE cut, however, greatly mitigates this issue.

In addition to the detailed study of morphology described in Sec. VI, we perform here a fit dividing the signal template into two independent templates, one with $|l| > |b|$ and the other with $|b| > |l|$. The former template favors the Galactic Plane, while the latter contains the *Fermi* Bubbles. As previously, the fit also includes a single template for the Bubbles in addition to the *Fermi* diffuse model and a isotropic offset. The extracted spectra of the signal templates are shown in Fig. 19. For energies below 10 GeV, where the claimed signal is present, they both show a clear spectral feature with consistent shape and normalization.

Appendix C: Sensitivity of the Spectral Shape to the Assumed Morphology

In our main analyses, we have derived spectra for the component associated with the dark matter template assuming a dark matter density profile with a given inner slope, γ. One might ask, however, to what degree uncertainties in the morphology of the template might bias the spectral shape extracted from our analysis. In Fig. 20, we plot the (central values of the) spectrum found for the dark matter template in our Inner Galaxy analysis, for a number of values of γ. The shapes of the spectra are highly consistent, almost entirely independent of this choice, for energies above 600 MeV, although they diverge at lower energies. For the range of slopes favored by our fits ($\gamma = 1.2 - 1.3$), however, the extracted spectra are always consistent within the 1σ error bars. We note that this conclusion is also true for the data without additional cuts on CTBCORE, although the degree of variation in the spectra below 600 MeV is considerably greater in that case.

Appendix D: Modeling of Background Emission in the Inner Galaxy

1. The *Fermi* Bubbles

The fit described in Sec. IV is a simplified version of the analysis performed in Ref. [8], where the spectrum of the Bubbles was allowed to vary with latitude. From the results in Ref. [8], it appears that this freedom is not necessary – the spectrum and normalization of the Bubbles varies only slightly with Galactic latitude.

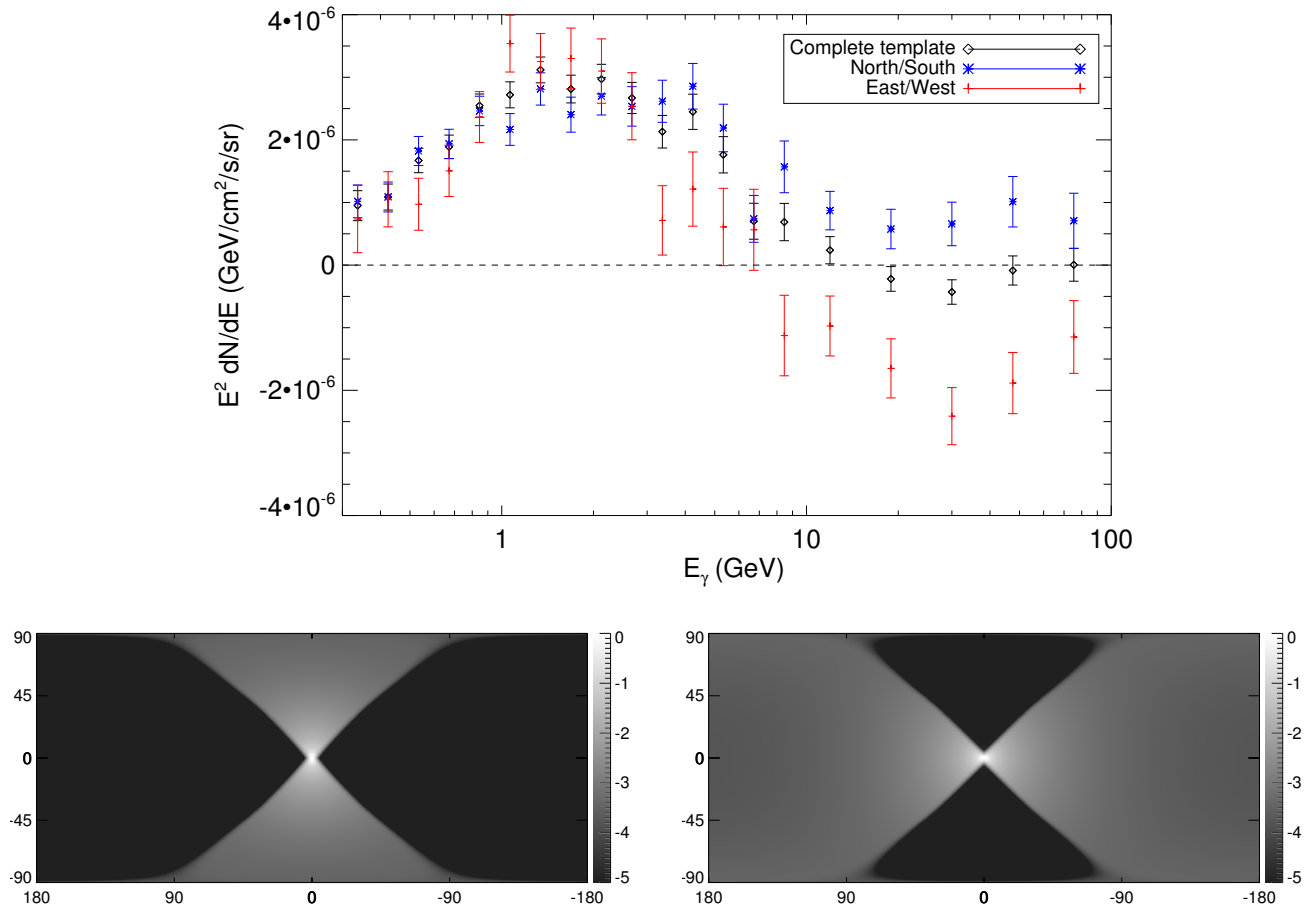

FIG. 19: In the upper frame, we show the spectra of the emission associated with the dark matter template, corresponding to a generalized NFW profile with an inner slope of $\gamma = 1.26$, as performed over three regions of the sky. Black diamonds indicate the spectrum extracted from the usual fit, whereas the blue stars and red crosses represent the spectra correlated with the parts of the template in which $|b| > |l|$ and $|b| < |l|$, respectively (when the two are allowed to vary independently). The corresponding spatial templates are shown in the lower row, in logarithmic (base 10) units, normalized to the brightest point in each map.

It is straightforward to reintroduce this freedom, and we show in Fig. 21 the spectrum correlated with the dark matter template if this is done. Above 0.5 GeV, the spectrum of the excess is not significantly altered by fixing the Bubbles to have a single spectrum. (Below 0.5 GeV, the spectrum of the lowest-latitude component of the Bubbles is driven negative, raising the spectrum correlated with the dark matter template.)

2. The Choice of Diffuse Model

Throughout our Inner Galaxy analysis, we employed the `p6v11` diffuse model released by the *Fermi* Collaboration, rather than the more up-to-date `p7v6` model. As noted earlier, this choice was made because the `p7v6` model contains artificial templates for the *Fermi* Bubbles and other large-scale features (with fixed spectra), making it more difficult to interpret any residuals.

Having shown that a single flat-luminosity template for the Bubbles is sufficient to capture their contribution without biasing the spectrum of the signal template, one might also employ the `p7v6` model in *addition* to an independent template for the Bubbles, in order to absorb any deviations between the true spectrum of the Bubbles and their description in the model. Unfortunately, the template for the *Fermi* Bubbles employed in constructing the `p7v6` diffuse model (which is not separately characterized from the overall Galactic diffuse emission) is different to the one employed in our analysis, especially in the regions close to the Galactic plane. Consequently, this approach gives rise to residuals correlated with the spatial differences between these templates. We find that the fits including the `p6v11` diffuse model plus the Bubbles are preferred at high significance over fits including the `p7v6` model plus the Bubbles, perhaps because of this issue.

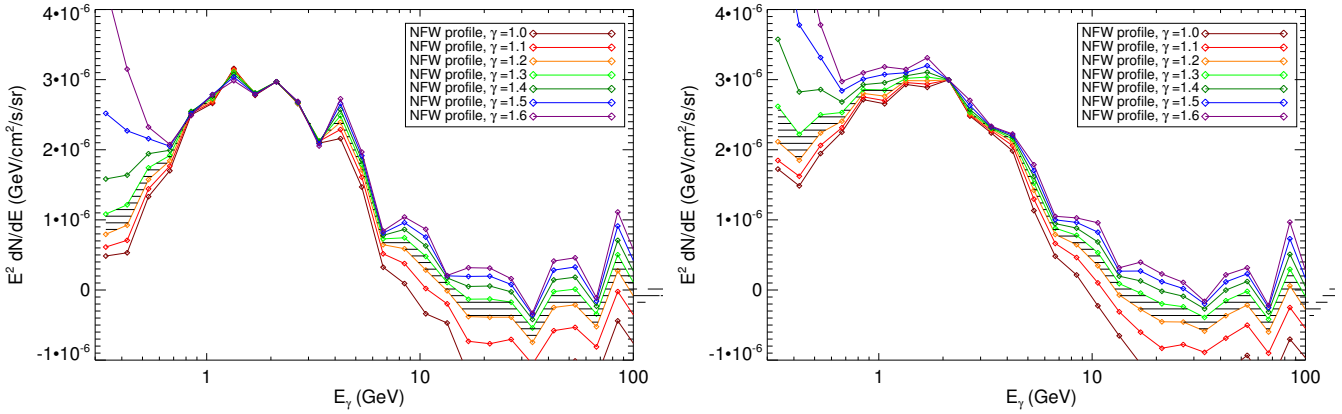

FIG. 20: The central values of the spectra of the dark matter templates for different values of the dark matter profile's inner slope, γ. To better facilitate comparison, each curve has been rescaled to match the $\gamma = 1.0$ curve at 2 GeV. All fits have been performed with the `p6v11` *Fermi* diffuse model, a single flat template for the Bubbles, and the dark matter signal template. The region between the $\gamma = 1.2$ and $\gamma = 1.3$ lines is cross-hatched. Error bars are not shown to avoid cluttering the plot. The spectra are remarkably consistent over the range of $0.5 - 10$ GeV, where the excess is most bright. The left panel shows results using our standard data selection, while in the right panel the additional cuts on CTBCORE were omitted.

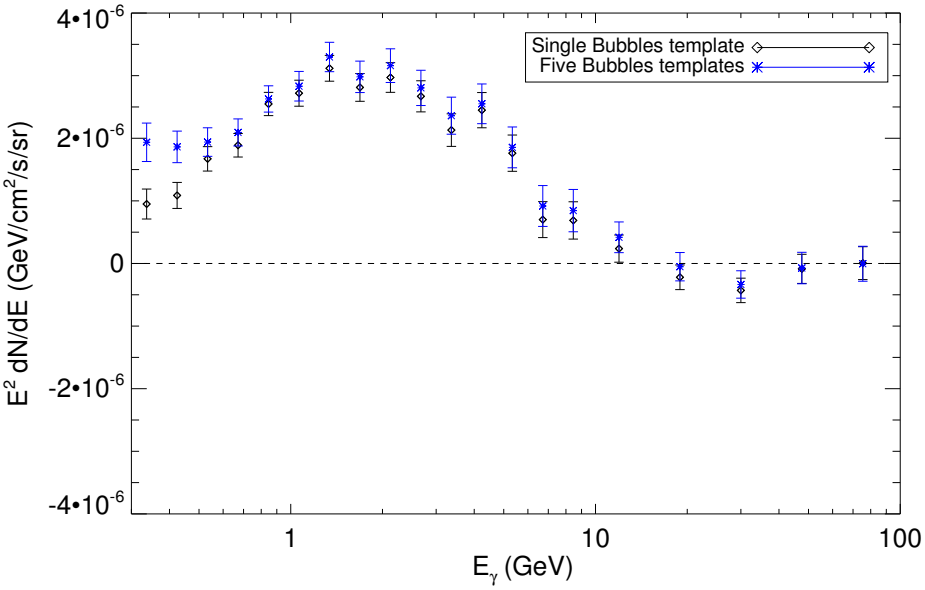

FIG. 21: The spectrum of the emission correlated with a dark matter template, corresponding to a generalized NFW profile with an inner slope of $\gamma = 1.26$, obtained by a fit containing either a single template for the *Fermi* Bubbles (black diamonds) or five templates for 10-degree-wide slices in Galactic latitude through the Bubbles (blue stars). The latter allows the spectrum of the *Fermi* Bubbles to vary with Galactic latitude.

For this reason, we employ the `p6v11` diffuse model for our principal analysis. However, using the `p7v6` model does not quantitatively change our results – the largest changes in the spectrum correlated with the dark matter template are actually above 10 GeV, where a slightly negative spectrum is replaced with slightly positive values. A direct comparison of these two results is shown in Fig. 22.

In Fig. 23, we compare the regions of the dark matter mass-annihilation cross section plane (for annihilations to $b\bar{b}$) that are best fit by the spectrum found in our default Inner Galaxy analysis (using the Pass 6 Galactic diffuse model, and fit over the entire sky, $|b| > 1^\circ$), to that found for the spectra shown in Figs. 19 and 22. In each of these variations, the resulting fit is significantly worsened relative to that found using the Pass 6 diffuse model and fit over the entire sky. However, the excess is still clearly present and consistent with a dark matter

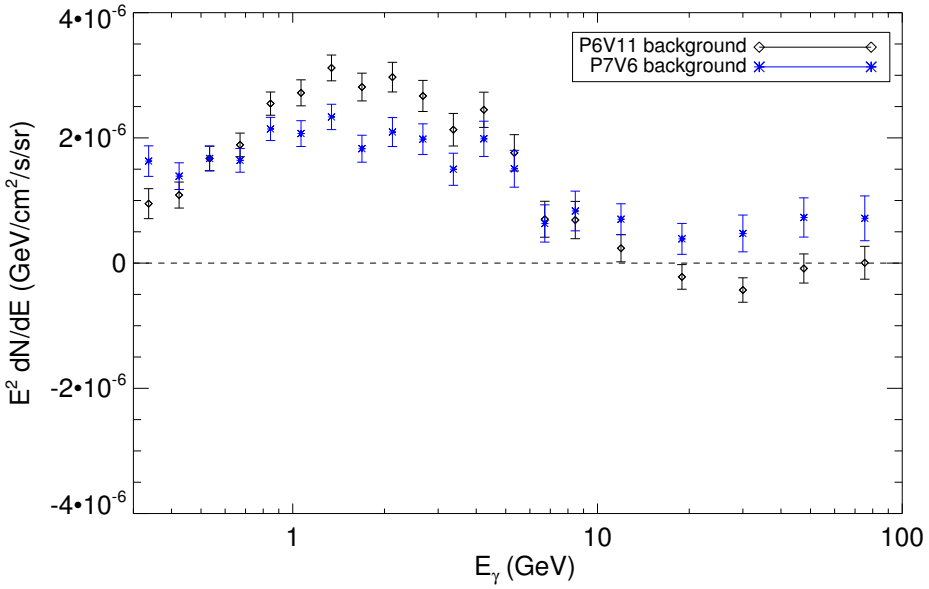

FIG. 22: The spectra of the emission correlated with a dark matter template, corresponding to a generalized NFW profile with an inner slope of $\gamma = 1.26$, with the background modeled by the `p6v11` diffuse model (black diamonds) or the `p7v6` diffuse model (blue stars). In both cases, the fit also contains an isotropic offset and a template for the *Fermi* Bubbles.

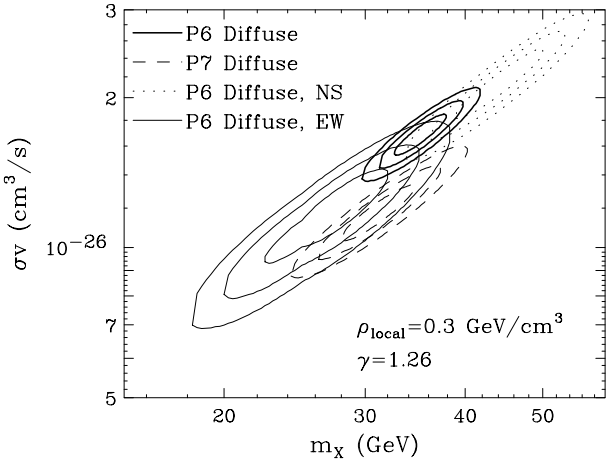

FIG. 23: A comparison of the regions of the dark matter mass-annihilation cross section plane (for annihilations to $b\bar{b}$) best fit by the spectrum found in our default Inner Galaxy analysis (using the Pass 6 Galactic diffuse model, and fit over the entire sky, $|b| > 1^\circ$), to that found for the spectra shown in Figs. 19 and 22. See text for details.

interpretation, and the qualitative results do not change with choice of diffuse model.

3. Variation in the π^0 Contribution to the Galactic Diffuse Emission

Although the spectrum of the observed excess does not appear to be consistent with gamma rays produced by interactions of proton cosmic rays with gas, one might wonder whether the *difference* between the true spectrum and the model might give rise to an artificially peaked spectrum. While we fit the spectrum of emission correlated with the *Fermi* diffuse model from the data, the model contains at least two principal emission components with quite different spectra (the gamma rays from the inverse Compton scattering of cosmic-ray electrons, and those from the interactions between cosmic-ray protons and gas), and their ratio is essentially fixed by our choice to use a single template for the diffuse Galactic emission (although we do allow for an arbitrary isotropic offset). Mismodeling of the cosmic-ray spectrum or density in the inner Galaxy could also give rise to residual differences between the data and model.

As a first step in exploring such issues, we consider relaxing the constraints on the background model by adding the Schlegel-Finkbeiner-Davis (SFD) map of interstellar dust [82] as an additional template. This dust map has previously been used effectively as a template for the gas-correlated gamma-ray emission [41, 42]. By allowing its spectrum to vary independently of the *Fermi* diffuse model, we hope to absorb systematic differences between the model and the data correlated with the gas. While the approximately spherical nature of the observed excess (see Sec. VI) makes the dust template unlikely to absorb the majority of this signal, if the spectrum of the

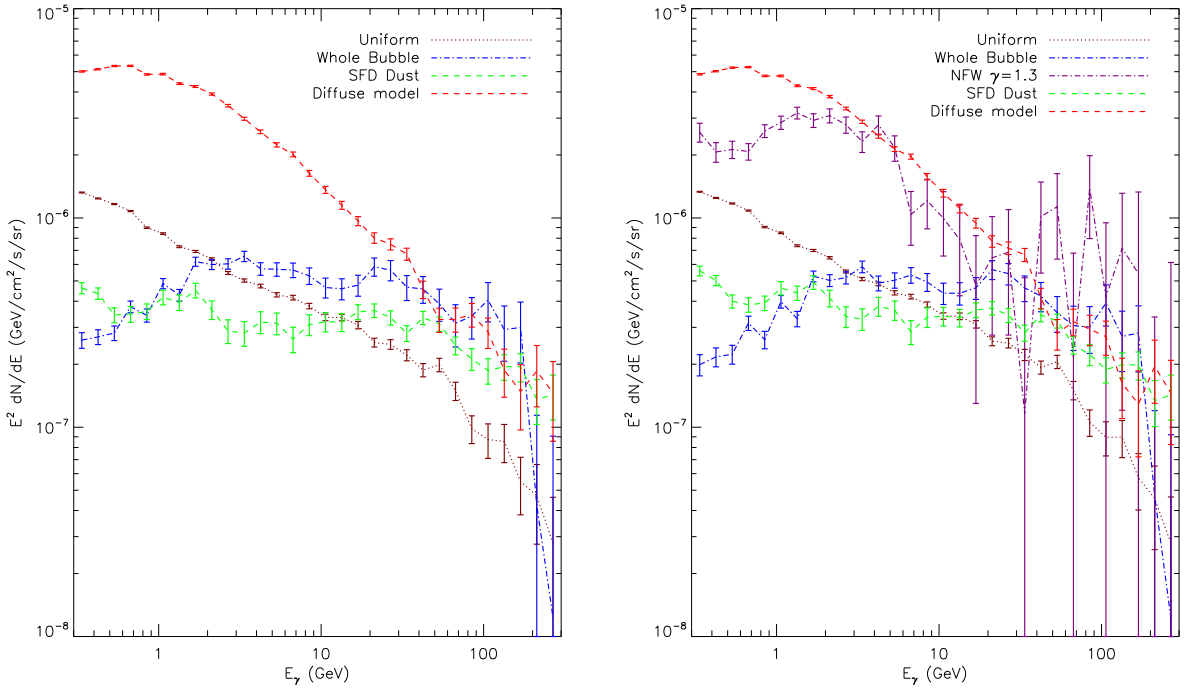

FIG. 24: In the left frame, we show the spectra resulting from a template fit with the usual backgrounds as well as the Schlegel-Finkbeiner-Davis dust map. The right frame shows the results of the same fit, but also including a dark matter template (with $\gamma = 1.3$).

excess were to change drastically as a result of this new component, that could indicate a systematic uncertainty associated with the background modeling.

In Fig. 24, we show the results of a template fit using the three background templates described in Sec. IV, as well as the SFD dust map. The additional template improves the fit markedly, and absorbs significant emission across a broad range of energies. However, when the dark matter template is added, the fit still strongly prefers its presence and recovers the familiar spectrum peaked at ∼1-3 GeV.

4. Modulating the π^0 Contribution

The use of the SFD dust map as a tracer for the emission from cosmic-ray proton interactions with gas (producing neutral pions) is predicated on the assumption that the distribution of cosmic-ray protons is approximately spatially uniform. In this appendix, we demonstrate the robustness of the observed signal against the relaxation of this assumption. Specifically we consider an otherwise unmotivated modulation of the gas-correlated emission that seems most likely to be capable of mimicing the signal: the proton density at energies of a few tens of GeV increasing toward the Galactic Center in such a way as to produce the spatially concentrated spectral feature found in the data. Since the gas density is strongly correlated with the Galactic Disk while the signal appears to be quite spherically symmetric (see Sec. VI), this would require the modulation from varying the cosmic-ray proton density to be aligned perpendicular to the Galactic Plane.

To this end we created additional templates of the form:

$$\text{Modulation} = (\text{SFD dust map}) \times \frac{f(r)}{g(r)}, \qquad \text{(D1)}$$

where $f(r)$ is a projected squared NFW template and $g(r)$ is a simple data-driven characterization of how the SFD dust map falls off with increasing galactic latitude and longitude. In this sense we have factored out how the dust map itself increases towards the Galactic Center and replaced this with a slope that matches a generalized NFW profile. Different modulations were generated by varying $f(r)$, which was done by choosing various values of the NFW inner slope, γ, from 0.5 to 2.0 in 0.1 increments. In order to determine $g(r)$, the dust map was binned in longitude and latitude and a rough functional form was chosen for each. For longitude, we analyzed the region with $|l| < 70^\circ$, and fit the profile of the dust map with a Gaussian. For latitude, we considered $|b| < 45^\circ$ and determined a best-fit using a combination of an exponential and linear function. These two best-fits were then multiplied to give $g(r)$. Each of the new templates were normalized such that the average value of all pixels with an angle between 4.9 and 5.1 degrees from the Galactic Center was set to unity. This was done in order

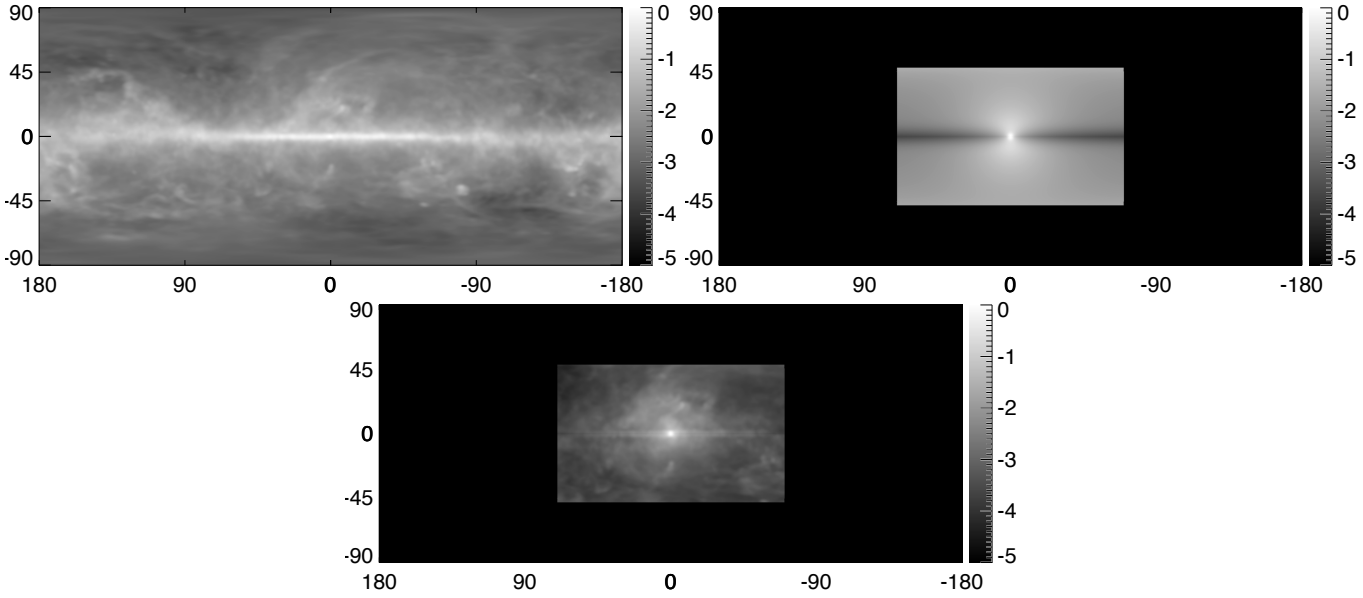

FIG. 25: Upper left frame: The Schlegel-Finkbeiner-Davis dust map, used as a tracer for emission from proton-gas interactions. Upper right frame: The $f(r)/g(r)$ modulation map created for an $f(r)$ associated with a generalized NFW profile with an inner slope of $\gamma = 1.1$. Lower frame: An example of a dust-modulation template, created by multiplying the dust map by the $f(r)/g(r)$ shown in the upper right panel. All maps are given in logarithmic (base 10) units, normalized to the brightest point in each map. The modulated-dust template is artificially set to zero for $|b| > 45^\circ$ and $|l| > 70^\circ$, to avoid errors due to the denominator factor becoming small; as it is already quite faint in these regions, this should not affect our results. See text for details.

to aid a comparison with the projected squared NFW template, which is normalized similarly. An example of the steps towards a final template is shown in Fig. 25, which was created using an $f(r)$ with $\gamma = 1.1$.

Each of the modulated-dust templates was combined with the three background templates described in Sec. IV and run through the maximum likelihood analysis. The results can be seen in the left frame of Fig. 26. Generically, the modulated-dust template acquires an appreciable coefficient in a similar energy range to the observed excess. (This should not be surprising, as the modulated-dust templates have been designed to absorb the excess to the greatest degree possible.) The spectrum associated with the template fit using an $f(r)$ of $\gamma = 1.1$, near where the χ^2 was improved most, is shown in the left frame of Fig. 27. Nevertheless, when a dark matter template was added to the analysis, there was always a substantial improvement in quality of the fit, as shown in the right frame of Fig. 26 for a dark matter template with an inner slope of $\gamma = 1.3$. Furthermore, the fit always associates the $\sim$GeV spectral feature with the dark matter template, in preference to the modulated dust map; an example of this is shown for $f(r)$ with $\gamma = 1.1$ in Fig. 27.

The above conclusions were checked to be robust against the choice of dataset (full, Q2 or Q1), as well as in the choice of the Pass 6 or Pass 7 *Fermi* diffuse model. As such, we suggest that even if the π^0 background has been modeled incorrectly, this deficiency is unlikely to provide an explanation for the observed signal. We find no evidence that the signal is correlated with the gas, even when allowing for an arbitrary modulation of the cosmic-ray density to maximize the similarity of the gas-correlated emission to a dark-matter-like signal.

Appendix E: Variations to the Galactic Center Analysis

In the default set of templates used in our Galactic Center analysis, we have employed astrophysical emission models which include several additional components that are not included within the official *Fermi* diffuse models or source catalogs. These include the two point sources described in Ref. [45] and a model tracing the 20 cm synchrotron emission. In models without a dark matter contribution, these structures are extremely significant; the addition of the 20 cm template is preferred with $\Delta\chi^2$=130, and the inclusion of the additional two point sources is favored with $\Delta\chi^2$=15.9 and 59.3, respectively.

Upon including the dark matter template in the fit, however, the significance of these additional components is lessened substantially. In this fit, the addition of the 20 cm template and the two new point sources is preferred at only $\Delta\chi^2$=12.2, 21.8, and 14.6, respectively. Additionally, our best-fit models attribute extremely soft spectra to each of these sources. The 20 cm component has a hard spectrum at low energies but breaks to a spectral index of -3.3 above 0.6 GeV. The spectral indices of the two point sources are -3.1 and -2.8, respectively. The

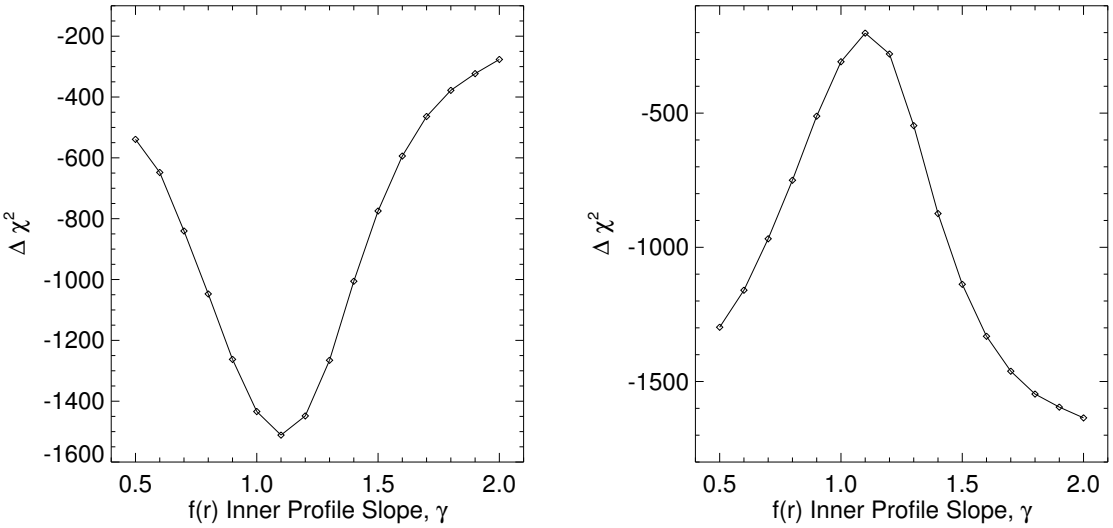

FIG. 26: In the left frame, we plot the change in the χ^2 between the template fit performed using known backgrounds and a modulated Schlegel-Finkbeiner-Davis dust map, and the fit using only the known backgrounds, as a function of the inner profile slope γ of the $f(r)$ template used in constructing the modulation. In the right frame, we show the χ^2 of the fit including the background model, modulated dust map, *and* a $\gamma = 1.3$ dark matter template, relative to the fit containing only the backgrounds and the modulated dust map, as a function of the inner profile slope γ of the $f(r)$ template.

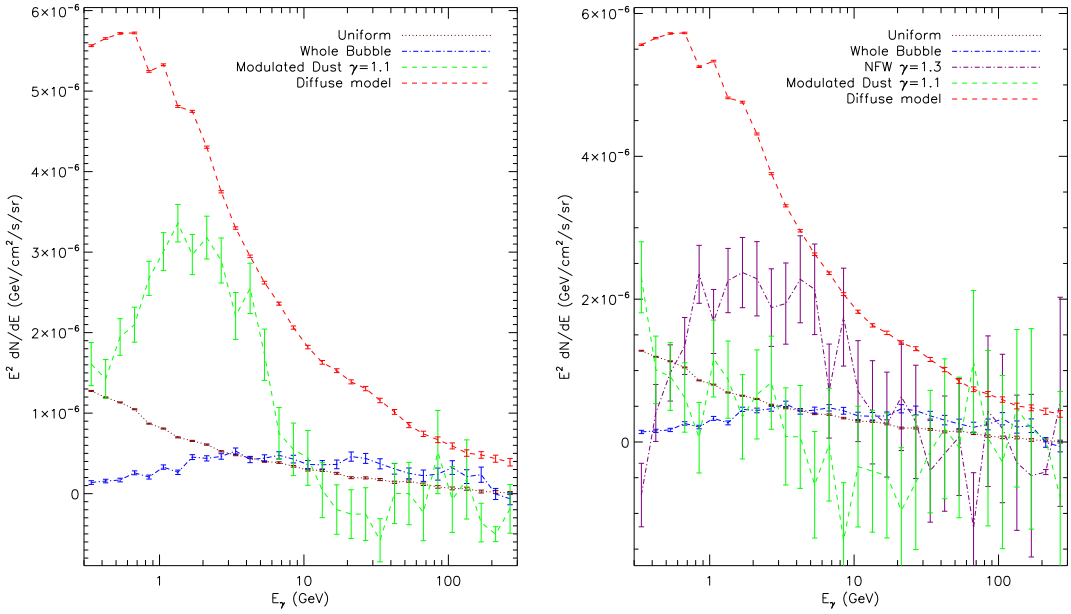

FIG. 27: The left frame shows the spectra obtained from a template fit employing the standard backgrounds and a modulated dust map, choosing $f(r)$ with $\gamma = 1.1$. In the right frame, we plot the coefficients from the same template fit, but with an additional $\gamma = 1.3$ dark matter template included.

total improvement in $\Delta\chi^2$ for the addition of these combined sources is 47.6.

In the left frame of Fig. 28, we compare the spectrum of the dark matter template found in our default analysis to that found when the 20 cm template and two additional point sources are not included (for $\gamma = 1.3$). The exclusion of these additional components from the fit leads to a softer spectrum at energies below ∼1 GeV, but does not influence the spectrum or intensity of the dark matter residual at higher energies.

In our default Galactic Center analysis, the isotropic emission is taken to follow a power-law form, while the

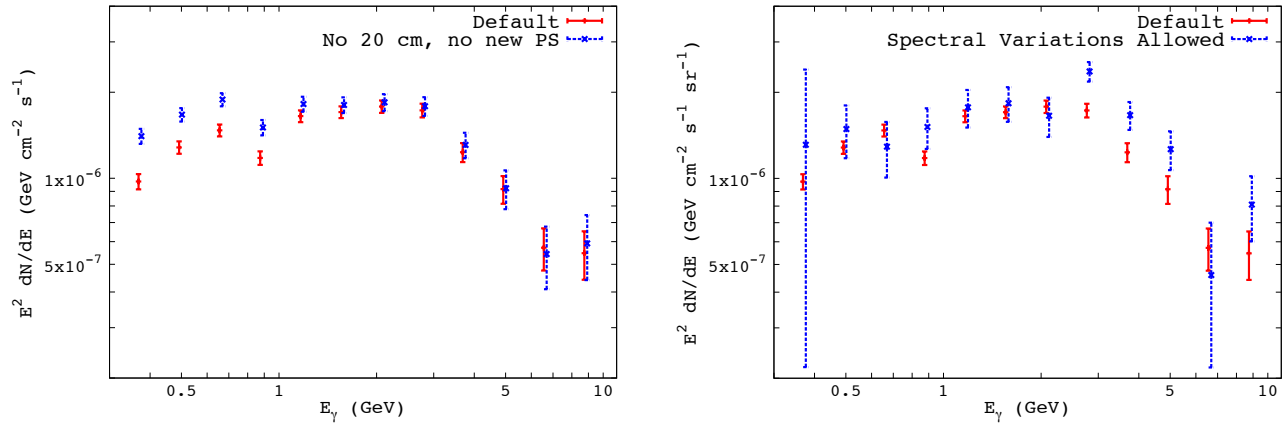

FIG. 28: Left frame: A comparison of the spectrum of the dark matter template found in our default Galactic Center analysis to that found when the 20 cm template and two additional point sources are not included in the fit (for $\gamma = 1.3$). The exclusion of these additional components from the fit leads to a softer spectrum at energies below $\sim$1 GeV, but does not influence the spectrum or intensity of the dark matter residual at higher energies. Right frame: The spectrum of the dark matter template found in our Galactic Center analysis under our default assumptions, and when the flux in each energy bin is allowed to float freely for each of the isotropic, 20 cm, and Galactic diffuse components. Although the error bars become larger when this additional freedom is allowed, the residual excess remains and is robust across a wide range of energies. See text for details.

emission associated with the 20 cm template is allowed to follow a broken power-law, and the Galactic diffuse model adopts a spectrum as given by the model provided by the *Fermi* Collaboration. As a test of the robustness of our results to these assumptions, we perform our fit once again, allowing the flux in each energy bin to float freely for each of the isotropic, 20 cm, and Galactic diffuse components. In the right frame of Fig. 28, we compare the spectrum extracted in this exercise to that found using our default assumptions. Although the error bars become larger, the residual excess is found to be robust across a wide range of energies.

Lastly, to explore the possibility that the gas distribution as implicitly described by the diffuse model has a systematically biased radial distribution, we performed our fits after distorting the morphology of the diffuse model template such that it becomes brighter at a higher or lower rate as one approaches the center of the Galaxy. However, we found this variation to yield no significant improvement in our fits.